PLASMODIUM EXOERYTHROCYTIC PARASITES REDIRECT TRAFFICKING OF HUMAN PROTEINS TO THE PARASITOPHOROUS VACUOLE

Jaeson Calla[1], Nimisha Mittal[1], Greg LaMonte[1], Benjamin Liffner[2], Karla P. Godinez-Macias[1], Krypton Carolino[1], Gregory T. Walker[1], Bing Yu Zou[1], Emma Paytas[1], Layné Guerra[3], Carlos Tong-Rios[3], Brice Campo[4], Joseph M. Vinetz[3,5], Dionicia Gamboa[3], Manuela Raffatellu[1,6,7], Sabrina Absalon[2], and Elizabeth A. Winzeler[1]

Affiliations:

[1]Department of Pediatrics, Division of Host-Microbe Systems & Therapeutics, School of Medicine, University of California, San Diego, La Jolla, United States of America.

[2]Department of Pharmacology and Toxicology, Indiana University School of Medicine, Indianapolis, United States of America.

[3]Laboratorio ICEMR-Amazonia, Laboratorios de Investigación y Desarrollo, Facultad de Ciencias y Filosofía, Universidad Peruana Cayetano Heredia, Lima, Peru.

[4]Medicines for Malaria Venture, Geneva, Switzerland.

[5]Current address: Department of Internal Medicine, Section of Infectious Diseases, School of Medicine, Yale University, New Haven, United States of America.

[6]Center for Microbiome Innovation, University of California San Diego, La Jolla, United States of America.

[7]Chiba University-UC San Diego Center for Mucosal Immunology, Allergy, and Vaccines (CU-UCSD cMAV), La Jolla, United States of America.

To whom correspondence should be addressed: ewinzeler@health.ucsd.edu

KEYWORDS

Hypnozoite, malaria, *P. vivax*, Hepatocyte

ABBREVIATIONS USED

PVR, Parasitophorous Vacuole Region; NR4A3, Nuclear receptor subfamily 4 group A member 3, HCI, High Content Imaging; qRT-PCR quantitative Reverse Transcriptase Polymerase Chain Reaction; ATQ, Atovaquone; EEF, Exoerythrocytic form; FC, flow cytometry; FACS, Fluorescence-Activated Cell Sorting; hpi, hours post infection; TRAP, Thrombospondin Related Anonymous Protein; GOLGA8A, Golgin subfamily A member 8A; MUC13, Mucin 13; CGA, Glycoprotein hormones alpha chain; Binding immunoglobulin protein, BiP; CXCL2, Chemokine

35 (C-X-C Motif) Ligand 2; CSP, Circumsporozoite protein; UIS4, Up-regulated in infective
36 sporozoites gene 4; Lipopolysaccharide, LPS.

ABSTRACT

Changes in host cell morphology and transcription after apicomplexan parasite infection have long been noted, but there have been few studies of the functional consequences of host cell remodeling. Here we show, using time-dependent immunofluorescence microscopy of multiple human cell lines (HFF, HepG2, HC-04, Huh7.5.1 and primary human hepatocytes), infected with multiple *Plasmodium* species (*Plasmodium berghei, P. falciparum* and *P. vivax* (hypnozoites and schizonts)), and antibodies to multiple human proteins (HsNR4A3, HsMUC13, HsGOLGA8A, HsCGA, HsBiP, HsCXCL2), that human protein trafficking is extensively modified in *Plasmodium* infected cells. Using conventional as well as ultrastructure expansion immunofluorescence microscopy we show that newly-synthesized human proteins are trafficked to the parasitophorous vacuole instead of the infected-cell plasma membrane, nucleus or extracellular space. Universal redirection of human signaling proteins cells the parasitophorous vacuole may provide a mechanistic explanation for how apicomplexan parasites can block host cells response to infection.

INTRODUCTION

Malaria remains a worldwide problem with up to 241 million cases reported in 2021[1]. Given the economic and humanitarian burden of malaria, and the continual emergence of parasite resistance to drugs that act against the symptomatic stages of the infection, new strategies to treat, prevent or control malaria are needed.

Liver cells are the primary cellular target of the *Plasmodium* parasite's exoerythrocytic stage. After injection into the vertebrate host by the bite of an infected Anopheline mosquito, the parasites (sporozoites) travel to the liver where they migrate and cross through several barriers. These barriers include endothelial cells, dermal fibroblast, liver sinusoidal endothelial cells (LSECs) and highly phagocytic Kupffer cells, that allows sporozoites to pass all barriers to find and infect hepatocytes[2,3]. When a suitable hepatocyte is reached, they inject the contents of their apical organelles using their specialized secretory organelles, the micronemes and rhoptries, into the hepatocyte membrane creating a molecular machine that enables the formation of a vacuole in the host cell cytoplasm[4]. The vacuole will enclose and protect the parasite and is surrounded by a

65 host-derived parasitophorous vacuole membrane (PVM)[5]. Similar vacuoles are formed when
66 blood stage malaria parasites invade erythrocytes and by other apicomplexan parasites, including
67 *Toxoplasma gondii* when they invade fibroblasts, for example[6]. Some malaria parasite species can
68 also remain in the liver in an inactive or dormant state, called a hypnozoite[7]. Hypnozoite-forming
69 species, especially *P. vivax*, represent barriers to malaria eradication because if they are not
70 eliminated by drug treatment, they can reawake months to years later, leading to patient relapse,
71 as well as active malaria transmission in an area that was once cleared of malaria. Despite their
72 importance, hypnozoites are poorly understood.

73 There are no clinical symptoms associated with liver stage infection[8]. Fever and chills that
74 are characteristic of malaria only develop after the merozoites are released from the schizont and
75 move to the circulatory system scanning for their next target cells, the erythrocytes.

76 Pre-erythrocytic stages are the primary target for the development of malaria vaccines. It
77 has been suggested that vaccines directed at this stage will be more effective because they will
78 suppress the spread of vaccine-resistance because of low parasite numbers at this stage (hundreds
79 versus billions in blood stages) and the only licensed vaccine, RTS, S/AS01, Mosquirix™, consists
80 of a target, circumsporozoite protein (CSP), which is highly expressed in *Plasmodium*
81 sporozoites[9-11]. Irradiated sporozoites also provide strong protection against malaria and have been
82 used in vaccine trials[12-14]. Irradiated sporozoites invade hepatocytes, form a trophozoite, but then
83 the host cell will apoptose before merozoite maturation is complete, allowing the display of
84 antigens and potentially elicit an improved immune response that is missing with unirradiated
85 sporozoites[15]. Vaccination with parasites that have mutations in PV-localized UIS3 and UIS4
86 result in an unprotective infection and sterile protection against challenge[16].

87 In the course of their development, erythrocytes will have shed many of their organelles,
88 including their nuclei, before they become susceptible to invasion by malaria parasites.
89 Hepatocytes, on the other hand, have nuclei and remain transcriptionally active after parasite
90 invasion. We had previously performed a dual RNAseq study on flow-sorted, *P. berghei*-infected
91 liver cells[17]. The experiments, which were conducted in a variety of time points and on different
92 cell types showed concerted patterns of gene upregulation, including genes involved in the immune
93 response, such as the mucin, *HsMUC13*[17]. Curiously, we observed that HsMUC13 protein

94 colocalized with parasite UIS4, a protein inserted into the parasitophorous vacuole membrane in
95 infected cells[17]. To further investigate these phenomena, here we examine other human genes that
96 were upregulated after parasite infection, including the orphan human nuclear hormone receptor,
97 *HsNR4A3*.

98 Surprisingly, we find that the cognate protein for all upregulated human genes that we
99 examine show colocalization with the parasite parasitophorous vacuole (PV) marker, UIS4[18]. We
100 show this colocalization is observed not only for *P. berghei* and *P. falciparum* liver stages, but for
101 both *P. vivax* schizonts and hypnozoites as well. Furthermore, using ultrastructure expansion
102 microscopy, a recently developed sample preparation method that enabled the isotropic expansion
103 of *Plasmodium* parasites up to 4.5-fold[19], we revealed the association of HsNR4A3 proteins with
104 the parasitophorous vacuole membrane (PVM) of *P. berghei* parasite. Our data indicate that in all
105 these parasites, host proteins are being redirected to the PV. We propose that apicomplexan
106 parasites manipulate host secretion apparatus to favor their development and to hide from the
107 immune system.

108 RESULTS

109 *Host proteins are transcriptionally upregulated during P. berghei infection of liver cells*

110 A previous dual (parasite and human) RNA-seq study with the rodent malaria parasite, *P.*
111 *berghei* (*Pb*GFP-SM$_{CON}$ (*Pb*-GFP)), identified a series of human transcripts that were upregulated
112 during parasite exoerythrocytic infection (Fig. 1a, 1b). Multiple time points, replicates, and
113 different hepatoma host cells (HepG2s, Huh7.5.1s, HC-04s) were used in these experiments in
114 which human cells were individually sorted into infected and noninfected pools based on the
115 presence of parasite-encoded GFP signal. Oddly, the most upregulated and statistically significant
116 genes across cell lines at 48 hours did not seem to be functionally related to one another. *HsMUC13*
117 encodes a secreted membrane localized mucin that is usually expressed in the gut. It is normally
118 upregulated after infection and is asymmetrically localized to luminal side of gut epithelial cells[20].
119 We had previously shown that it colocalized to the parasite vacuole in mature *P. vivax* and *P.*
120 *berghei* schizonts[17]. Also upregulated in multiple hepatocyte-derived lines was *HsNR4A3* ($p = 2.8 \times 10^{-30}$).
121 The NR4A subfamily encodes orphan nuclear receptors that belong to the larger nuclear

122 receptors (NRs) superfamily of eukaryotic transcription factors. The NR4A subfamily includes
123 three members, namely NUR77 (HsNR4A1), NURR1 (HsNR4A2) and NOR1 (HsNR4A3), which
124 are gene regulators and participate in diverse biological functions. Although exact function of
125 HsNR4A3 is not known, data suggest a potential role in controlling glucose in some cell types[21].
126 NR4A3 knockout mice show expansion of the pancreatic beta cells, needed for insulin production,
127 and NR4A3 overexpression lines increase glucose production in response to some stimuli, and act
128 as activator of beta cell proliferation and insulin production[22,23]. It has also been reported as an
129 NLRP3 inflammasome activation-responsive gene[24]. In the cancer arena, it has been shown that
130 NR4A3 overexpression attenuates proliferation of cancer cells and promotes apoptosis by
131 augmenting the expression of pro-apoptotic genes via a p53 dependent mechanism[25]. *HsCGA*
132 (adjusted $p = 4.4\text{x}10^{-13}$) encodes the shared alpha chain of the heterodimeric human glycoprotein
133 hormones; thyrotropin/thyroid stimulating hormone/TSH, lutropin/luteinizing hormone/LH,
134 follitropin/follicle stimulating hormone/FSH and choriogonadotropin/CG. HsCGA, along with its
135 partner, would normally be secreted into the bloodstream where it would bind rhodopsin-like G
136 protein-coupled receptors on the target cell[26]. *HsCGA* is expressed at high levels in the placenta
137 but is also upregulated in breast cancer and is an estrogen receptor alpha (ERα)-responsive gene
138 in human breast tumors[27]. *HsTAS2R4* encodes a G-protein coupled receptor that is normally
139 expressed on the surface of tongue epithelial cells. It is responsive to bitter molecules, including,
140 interestingly, the antimalarial, quinine but may also play a role in small molecule-sensing in
141 extraoral cell types[28].

142 In addition, the set of statistically significant upregulated genes included several noncoding
143 genes. The lncRNA, *HsNEAT1* (adjusted $p = 1.8\text{x}10^{-34}$), promotes activation of inflammasomes in
144 macrophages[29]. *HsMALAT1*, also known as *HsNEAT2* is also a large, non-coding RNA, which is
145 highly conserved amongst mammals and highly expressed. Overexpression of *HsMALAT1*
146 suppresses breast cancer metastasis in transgenic, xenograft, and syngeneic models of cancer[30] and
147 is also strongly associated with inflammasome activation[31].

148 Because the RNAseq studies had been performed on model hepatoma cells lines we used
149 qRT-PCR to confirm the upregulation of *HsNR4A3, HsMUC13, HsCGA, HsSLC22A8,*
150 *HsMALAT1, HsRASSSF9, HsSDHA, HsSLC25A27, HsNEAT1,* and *HsTAS2R4* in *P. berghei*-
151 infected primary human hepatocytes, as well as in *P. berghei* infected Huh7.5.1, HepG2 and HC-

152 04 cells. Cells were infected with *P. berghei* expressing GFP and flow sorted. RNA was extracted
153 from infected cells, as well as from control, parallel non-infected cells. In these four cell lines, we
154 observed consistent 13-20-fold upregulation of *HsNR4A3* in all cell lines except for HepG2 cells
155 (Fig. 1c). We also observed upregulation of other transcripts via qRT-PCRs but not as consistently
156 across all lines.

157 To further ensure that the patterns were not specific to *P. berghei*, we performed Western
158 blot analysis. We obtained several commercial antibodies to some of the different human proteins
159 that showed the highest, most significant, and reproducible upregulation. These included
160 HsNR4A3, HsCGA, and HsMUC13. HsGOLGA8A, was also included (probability of
161 upregulation of chance = 4.04×10^{-10}). It encodes a member of the Golgin family of membrane
162 proteins which play a role in tethering vesicles to the Golgi apparatus[32,33]. All 21 annotated Golgins
163 were amongst the set of upregulated genes in infected cells, 13 significantly (hypergeometric mean
164 probability of enrichment by chance = 5.5×10^{-5}), with an average upregulation of 2.3×. The bulk
165 cultures as well as uninfected HC04 control cultures were infected with both *P. berghei* and *P.*
166 *falciparum*. All the evaluated antibodies showed recognition of a single band corresponding to the
167 native protein (Fig. S1a, S1b). The data also generally showed upregulation of the proteins in the
168 infected bulk cultures, although, as expected, upregulation was not as pronounced as observed
169 using flow-sorted cells, given the low number of infected cells (1 to 2%). The antibody to CGA1
170 recognized a larger than expected protein. CGA1 is heavily glycosylated which may contribute to
171 the size difference.

172 *Upregulated host proteins show colocalization with PVM via immunofluorescence analysis*

173 To understand the localization, we used immunofluorescence and confocal microscopy to
174 determine whether the RNA upregulation resulted in changes to protein expression. First, assays
175 were performed with *P. berghei*, the species on which hepatocyte flow sorting was performed,
176 using mature parasites. Isolated *P. berghei* sporozoites were incubated with a permissive human
177 liver cell line, HC-04. After 48 hours, the cultures were fixed and stained with a set of primary
178 commercial antibodies against various upregulated hepatocyte proteins (HsNR4A3, HsCGA,
179 HsGOLGA8A, and HsMUC13), and to parasite UIS4 (Fig. 2a), a parasite protein highly expressed
180 in sporozoites and liver stages of multiple *Plasmodium* species, and which localizes to the

181 parasitophorous vacuole membrane in both hypnozoites and schizonts[34]. All antibodies (against
182 HsNR4A3, HsCGA, HsGOLGA8A, and HsMUC13 proteins) showed high expression of their
183 cognate proteins in *P. berghei*-infected but not -uninfected HC-04 cells. Interestingly, all four host
184 proteins colocalized with the parasite marker, UIS4 (Fig. 2a). NR4A3 is normally localized to the
185 nucleus[35] and indeed staining was observed in the nucleus in uninfected cells visible in the image.
186 GOLGA8A encodes protein with an N-terminal coiled-coil domain and a single C-terminal
187 transmembrane domain and is also known as golgin-67. It localized to the Golgi apparatus which
188 in most human cells is adjacent to the nucleus[36]. As expected, our staining showed weak
189 HsGOLGA8A surrounding the nucleus in uninfected cells. MUC13 and CGA are both expected
190 to be secreted into the extracellular space. Uninfected cells showed some weak diffuse cytoplasmic
191 staining with antibodies to these proteins.

192 To determine if similar staining would be observed in human cells infected with the human
193 pathogen, *P. falciparum,* we performed experiments using freshly dissected *P. falciparum*
194 sporozoites and primary hepatocytes. Sporozoites were placed on primary hepatocytes in 96-well
195 plates and cultures were incubated for 120 hours, necessary because of the longer *P. falciparum*
196 liver development time. Immunofluorescence was accomplished using a *P. vivax* antibody to
197 PvUIS4[34] (which is cross-reactive with PfUIS4) (Fig. 2b) and the same primary human antibodies.
198 These experiments confirmed upregulation of the HsNR4A3, HsCGA, HsGOLGA8A, and
199 HsMUC13 proteins with staining, as with *P. berghei*, occurring in the PVM region, overlapping
200 largely with UIS4 staining. Importantly, these data showed that the staining patterns were not
201 associated with the use of a hepatoma cell line and were conserved in primary human hepatocytes.

202 We next examined another human pathogen, *P. vivax,* which can remain in an infected
203 liver cell as a hypnozoite that can be activated months or years after the primary infection. As *P.*
204 *vivax* cannot be maintained in cell culture, patients diagnosed with *P. vivax* malaria, were recruited,
205 and asked to provide 20mL of whole blood, which was used to feed fasted, female *Anopheles*
206 *darlingi* mosquitoes using a standard membrane feeding assay. After 14 days the mosquitoes were
207 dissected to obtain sporozoites, which were used to infect HC-04 cell lines (see Methods). After
208 five days, the cells were fixed and stained with our primary antibodies (against HsNR4A3,
209 HsCGA, HsGOLGA8A, and HsMUC13 proteins). Again, all antibodies showed strong
210 colocalization with the parasites (Fig. 2c) for all proteins.

211 To determine whether this pattern would be observed for hypnozoites we searched for UIS4
212 positive objects that were smaller than 10µm and which showed characteristic circular patterns
213 associated with UIS4 signal, the bonafide way to identify hypnozoites[34]. For our *P. vivax* infected
214 samples, we identified hypnozoites at a rate of 1 per 5,000 hepatocytes, and schizonts at a
215 frequency of ~1:1,000, some of which are shown in Fig. 2d. Interestingly, the same
216 immunofluorescent micrographs also showed colocalization with HsNR4A3, HsCGA,
217 HsGOLGA8A, and the HsMUC13 (Fig. 2d). In fact, previous parasite-associated
218 immunolocalization had been observed for HsMUC13[17]. Analysis of the images showed a strong
219 correlation between UIS4 and the different tested proteins for all species (Fig. S2).

220 While the relocalization of one protein could be functional, the relocalization of all was
221 puzzling. To rule out cross hybridization or other antibody specific effects we next performed
222 staining with an antibody to the parasite cytosolic markers *P. berghei* and *P. vivax* HSP70 (*Pb-*
223 *Pv*HSP70)[17] in infected HC-04 cells (Fig. S3a) instead of UIS4. These micrographs showed similar
224 localization of the human proteins, ruling out the possibility of the species-specific secondary
225 antibodies cross-reacting with the primary UIS4 antibody. In addition, we repeated IFAs with a
226 variety of different antibodies using the *P. berghei* infection model and in all cases, the same
227 patterns were obtained (Figure S4).

228 *HsNR4A3 edited lines show decreased NR4A3 staining in Westerns and IFA*

229 To further assess the question of antibody specificity as well as HsNR4A3 functionality,
230 we next performed knockouts on *HsNR4A3*. We used CRISPR/*Cas9*-based methods to disrupt
231 *HsNR4A3* in clonal HC-04 cell lines using two different approaches (two plasmid or single
232 plasmid) and different guide RNA sets (Fig. S5a and S5b), obtaining six different stably edited
233 clones (GL1, GL2, and GL3 and NM1, NM2, and NM3 created using the two approaches)).
234 Western blot analysis showed lower expression of HsNR4A3 in five of six clones (clones GL1 and
235 GL3 and NM1, NM2, and NM3)) relative to native HC-04 cells (Fig. S5c, S5d).

236 To evaluate antibody specificity, *HsNR4A3* knockout cells were infected with *P. berghei*
237 (*Pb*-ANKA-GFP-Luc SMCON (*Pb*-Luc)) sporozoites. After 48hpi, the infected and uninfected
238 cells were evaluated by immunofluorescence and confocal microscopy. For HC-04 HsNR4A3
239 unmodified cells (WT) we observed colocalization with the parasite markers UIS4 (Fig. S5e) and

240 HSP70 (Fig. S5e, S5f). In contrast, no NR4A3 staining was observed in *HsNR4A3* knockout cells
241 (Fig. S5e) and pattern quantification showed no correlation ($p < 0.0005$) Fig. S5f). Staining was
242 similar to the negative control in which the NR4A3 antibody was not used. These data largely rule
243 out the possibility of NR4A3 antibody cross-hybridization with an as-yet unspecified parasite
244 protein.

245 To confirm our findings in *P. vivax*, we also performed *in vitro* infection tests using cloned
246 GL1 and GL3 *HsNR4A3* knockout cells and *P. vivax* parasites obtained as described above. We
247 observed a marked expression of the HsNR4A3 protein in the HC-04 HsNR4A3 WT cells in the
248 two stages of the parasite (hypnozoites and schizonts) showing the expected co-staining with UIS4.
249 For clone GL1, we did not identify any parasites (see below) while for clone GL3 (Fig. S5g), we
250 observed no signal or co-staining with UIS4. A statistically-significant loss of staining correlation
251 in *HsNR4A3* knockouts was confirmed by image quantitation (Fig. S5h, S5i).

252 *Role of the protein HsNR4A3 in exoerythrocytic infections*

253 To determine whether HsNR4A3 contributes to parasite growth and development we
254 investigated both schizont size, schizont number and schizont morphology in the *HsNR4A3*
255 knockout clones in *P. berghei* and *P. vivax*. First, *in vitro* infections with *P. berghei* parasites were
256 carried out. We performed a qRT-PCR experiment using primers to the *P. berghei* 18S RNA gene
257 as previously described[37]. These data showed that a higher number of cycles were needed to detect
258 parasites in NM1, NM2 and NM3 clones, with NM3 requiring almost as many cycles for detection
259 as treatment with 5nM atovaquone, a drug which completely blocks parasite exoerythrocytic
260 development (Fig. S6a). Next, high content imaging analysis was performed on *P. berghei* infected
261 cells and used to determine the number of UIS4 positive objects per field ($0.8cm^2$). These data
262 showed a ~70% reduction in the relative number of parasites in all three *HsNR4A3* knockout clones
263 (Fig. S6b). We also observe that most of the positive objects identified in *HsNR4A3* knockout cells
264 (NM1-NM3) have a diameter of 5µm compared with 40µm the WT HC-04 cells (Fig. S6c).

265 To investigate the role of HsNR4A3 in *P. vivax* development, we infected our GL1 and
266 GL3 *HsNR4A3* knockout lines with *P vivax* sporozoites, obtained as described above, and allowed
267 the parasites to develop for 120 hours. Cultures were co-stained with the UIS4 parasite marker to
268 identify and count infected cells. Hypnozoites were distinguished from schizonts based on parasite

269 size (Fig. S6d, S6e). In both clones we observed fewer schizonts, although the reduction in the
270 number of hypnozoites was not as marked. This suggests that the expression of the HsNR4A3
271 protein is needed for the *P. vivax* parasite to complete the schizont maturation process. To
272 determine if this was true for *P. berghei* as well, we also infected the *HsNR4A3* knockout clones
273 with GFP-expressing *P. berghei* sporozoites and performed flow sorting of GFP-positive objects
274 on GL1 and WT HC-04 cells after 48 hours incubation (Fig. S6f). We observed a marked reduction
275 in the number of GFP positive objects in GL1. These data suggest that HsNR4A3-depleted HC-04
276 cells may be less able to support parasite invasion and maturation but also highlight that different
277 clones have different levels of gene disruption in diploid human cells, and the phenotype is slightly
278 inconsistent. More work will be needed to determine the contribution of HsNR4A3 to parasite
279 development and to assess if both copies are disrupted or only one.

280 *HsNR4A3 is trafficked to the parasitophorous vacuole region during liver stage development*

281 As a nuclear hormone receptor, HsNR4A3 is expected to traffic between the nucleus and
282 cytoplasm. To study the temporal dynamics of HsNR4A3 relocalization in the context of a parasite
283 infection we next conducted a time course experiment in *P. berghei,* monitoring subcellular
284 localization of HsNR4A3 during exoerythrocytic infections. *P. berghei* sporozoites were placed
285 on HC-04 cells and samples were collected and fixed for immunofluorescence analysis every three
286 hours. At three hours, HsNR4A3 staining was observed in the host cell nucleus, overlapping with
287 host cell DAPI for both infected and uninfected cells, as expected for a nuclear hormone orphan
288 receptor, which are constitutively-active transcription factors (Fig. 3). In contrast, the parasite-
289 specific marker, UIS4, was clearly in the host cell cytoplasm, surrounding the parasite and only
290 found in infected cells. At later time points, HsNR4A3 was no longer found in the host nucleus,
291 and was now found in the cytoplasm of infected cells. By 18 hours, weak HsNR4A3 staining was
292 observed in the nucleus of uninfected cells, but strong staining was observed in infected cells in
293 the PVR. In late stages (24-96 hours), HsNR4A3 expression overlapped with the parasite marker,
294 UIS4 (Fig. 3a, 3b). Given the clear upregulation in NR4A3 gene expression in infected cells, these
295 patterns are consistent with newly synthesized NR4A3 being trafficked directly into the PVR
296 instead of to the host nucleus. Image quantification (Fig. S7a) showed little PbUIS4:HsNR4A3
297 correlation at early times (<0.1 at 3 hours) but strong correlation at later times (>0.9 at 96 hours),
298 and an inverse relationship with DAPI:HsNR4A3 correlation (Fig. S7b). Similar relocalization

299 patterns were also observed over the course of *P. berghei* exoerythrocytic development for
300 HsGOLGA8A (Fig. S8a, S8b) with the staining observed around the HC-04 cell nucleus at time
301 zero and then moving to co-localize with PbUIS4 by 48 hours in infected cells only. As a control,
302 we examined a gene that did not show differential regulation after infection. HsBiP, also known
303 as HsHSPA5 or GRP-78 is a highly expressed heat shock protein that is typically found in the
304 lumen of the ER and is a well-established marker of ER. It shows little evidence of differential
305 regulation after infection in our dual RNAseq study ($p = 0.97$, log2fold change = -0.006) but is
306 one of the most abundant transcripts (ranking at 96 of ~25,000 transcripts in terms of base mean
307 expression). Although in early stages of development it surrounded the host nuclei (Fig. S8c) as
308 predicted in all eukaryotic cells, it completely colocalized with PbUIS4 by 72 hours of infection
309 and image analysis showed strong correlation with PbUIS4 (Fig. S8d).

310 *Expansion immunofluorescence confocal microscopy localizes hsNR4A3 to the parasitophorous*
311 *vacuole.*

312 To further characterize the interaction of HsNR4A3 with the PVM we turned into
313 ultrastructure expansion microscopy (U-ExM) coupled with Airyscan super-resolution
314 microscopy[19,38]. We fixed and expanded Huh7.5.1. cells after 48 hours of infection with *P. berghei*
315 parasites. Previous work in blood-stage parasites demonstrated that the higher resolution achieved
316 post-expansion allows to distinguish the PVM from the parasite plasma membrane both stained by
317 Bodipy-TR-ceramide dye[38]. Using anti-UIS4 antibody in combination with Bodipy-TR ceramide
318 staining we expectedly localized UIS4 at the PVM and observed numerous UIS4-positive lipid-
319 enriched vesicles within the PV space or in the host-cytoplasm (Fig. S9). After the validation of
320 UIS4 as U-EXM compatible PVM marker, we used primary antibodies against HsNR4A3 and
321 UIS4 proteins and confirmed the close association of HsNR4A3 with the PVM. HsNR4A3
322 localized at the host-cytosolic side of the PVM in foci that predominantly are uniformly distributed
323 around the PV and occasionally concentrated in pockets associated with the PVM with some
324 staining in the PV (Fig. 4a).

325

326 *Secreted immune signaling molecules are also redirected to the PVR*

327 One unifying hypothesis that could explain the colocalization that was observed with many
328 of our examined proteins would be if all newly synthesized inter and intracellular host signaling
329 molecules were redirected away from their usual cytoplasmic or cell membrane location and into
330 the parasite vacuole membrane region PVM, potentially as a way to avoid immune signaling or
331 instructions to undergo apoptosis. To further investigate this, we examined the list of upregulated
332 genes to identify well-characterized cytokines and selected HsCXCL2 (Fig S10a, S10b), which
333 was expressed and upregulated in infected HC-04 cells in particular ($\log_2$ fold change = 2.76, p =
334 1.46×10^{-07}). *HsCXCL2* encodes a chemokine ligand that is secreted by monocytes and
335 macrophages at the site of inflammation and is strongly responsive to LPS stimulation. It binds to
336 the chemokine receptor, HsCXCR2 and plays a role in early stage of neutrophil recruitment during
337 tissue inflammation[39]. To test the hypothesis that HsCXCL2 would migrate to the PVR after
338 immune stimulation HC-04 cells were first infected with *P. berghei* and then after 24 hours treated
339 with LPS. Immunofluorescence assays using a CXCL2 antibody were performed at 2, 24 and 48
340 hours (26, 48 and 72hpi). These data showed a strong upregulation of CXCL2 expression in LPS-
341 treated, infected and uninfected HC-04 cells. As with other host proteins, HsCXCL2 staining
342 colocalized with the PVR and PbUIS4 in the infected cells (Fig. 5a, 5b). The specificity of
343 commercial antibodies against HsCXL2, HsBiP (Fig S11a) and the controls (Fig S11b) are
344 showed.

345 DISCUSSION

346 Here we have shown that five different upregulated proteins (HsNR4A3, HsCGA,
347 HsGOLGA8A, HsMUC13, and HsCXCL2), each with different, intracellular trafficking patterns,
348 all end up in the PV or PVR, surrounding the parasite. In addition, this pattern has also been
349 observed by others with unrelated proteins: Posfai and coworkers observed upregulation of
350 HsAQP3 in a *P. berghei* dual RNAseq study (this was confirmed in our dataset, $p = 1.81\text{x}10^{-19}$)
351 and also showed that this transporter is localized to the PVM[40]. Normally HsAQP3, a membrane
352 transporter of water and glycerol, would be trafficked to the human cell plasma membrane. The
353 host autophagosome marker, LC3, as well as other autophagosome markers, P62, NDP52, and

354 NBR1 and LAMP1 also colocalize with UIS4[41-45]. The timing of relocalization is also similar,
355 occurring here as early as 12 hours post infection, as observed for LC3[43]. While each protein that
356 was examined here and by others could have a distinct role in supporting parasite development,
357 we favor a model in which newly synthesized proteins are redirected to the vacuole and away from
358 their natural home, potentially as a universal neutralization mechanism to block cell signaling and
359 apoptosis in the infected host.

360 It has been proposed that one mechanism by which the malaria parasite may accomplish
361 the host cell remodeling is through modification of the host autophagy pathways[46]. Here the host
362 cell is relatively passive, and the parasite now directs the formation of lysosomes which are used
363 to capture pieces of the host cytoplasm and redirect them toward the parasite. This has been termed
364 the *Plasmodium*-associated autophagy-related (PAAR) response[46]. Support for this model comes
365 from the demonstration that many autophagosome markers colocalize with the PVM and some are
366 also needed for parasite development[46]. However, this does not explain why a variety of
367 completely unrelated proteins, including MUC13, AQP3[40], NR4A3 or CXCL2, all show the same
368 behavior. This model, which is based on what is observed in infected erythrocytes, does not
369 necessarily take into account the massive transcriptional changes which are observed in infected
370 hepatocytes. This autophagy model also suggests that lysosome cargo that is directed to the PV
371 consists of digested proteins.

372 We propose an alternative but possibly complementary model in which newly synthesized
373 host proteins are now secreted into the PV because the host secretion apparatus has been
374 extensively modified. This model is supported by the fact that many of the antibodies we have
375 used in our study are to full length proteins and their appearance in the PVR is associated with
376 their transcriptional upregulation in the infected host cells. Our model is also based on our
377 micrographs as well as those of others[47-49] showing that the endoplasmic reticulum (ER) is also
378 relocalized to the PVR. In fact, the upregulation and association of HsGOLGA8A with the PVR
379 may be a consequence of the relocalization of the ER and Golgi apparatus around the PV and may
380 be the easiest to understand in light of recent reports showing that the Golgi and ER move from
381 around the host nucleus in uninfected cells to around the parasite[47-49].

382 Most of the proteins that we examined bear signal sequences that would direct them to the
383 ER and Golgi. On the other hand, HsNR4A3, which presumably does not bear a signal sequence,

384 would normally be translated in the cytoplasm and imported to the nucleus via the nuclear pore
385 complex (NPC) by virtue of its nuclear localization signal. In early stages of the infection,
386 HsNR4A3 is found in the nucleus and only later relocates to the PV. Do nuclear pore proteins
387 somehow relocate from the nuclear membrane to the PVM? It is possible that nuclear pore complex
388 proteins find their way to the PVM, as well. It was recently shown that infection with LS parasites
389 results in the host microtubule organizing center (MTOC) relocalizing to the PVM. The authors of
390 the paper suggested that during infection MTOCs reorganize the host microtubule network around
391 the developing LS parasites[50]. It may be that there is an active contact site between the host nucleus
392 and the PVM through the NPCs. Active contact sites between nucleus and mitochondria[51] or
393 multiple inter-organelle contact sites[52] have been shown in mammalian cells.

394 Despite questions about how it occurs, the redirection of transcription factors away from
395 the host nucleus into to the PV could provide physiological advantages to the parasite. It could
396 render the infected cell less able to transcriptionally respond to external stimuli such as signals to
397 divide, differentiate, or undergo apoptosis, all of which would likely be unfortunate events for the
398 parasite. This could be particularly important for cells that must harbor hypnozoites for many
399 years. Although we do find that HsNR4A3 expression may help the parasites survive and grow,
400 we also noted that uninfected HsNR4A3 knockdown HC-04 cells appear to initially grow faster
401 which could alter the final ratio of infected to uninfected cells, which could contribute to lower
402 relative parasite numbers after a 48-hour incubation. We observed 3 to 6 × more edited by
403 CRISPR/*Cas*9 NM1 and NM3 cells in comparison to the HC-04 HsNR4A3 WT cells 36 hours
404 after plating. In fact, HsNR4A3-edited human breast and lung cancer cells (MDA-MB-231 and
405 H1299, respectively) show increased cell proliferation[25]. The redirection of HsNR4A3 away from
406 the nucleus could also have consequences for immune evasion. Proliferation and IL-2 production
407 levels of T cells cocultured with HsNR4A3 knocked-down DCs were significantly lower than that
408 of T cells cocultured with control DCs[53].

409 In contrast, HsCGA, HsMUC13, and HsCXCL2 are all secreted proteins (one membrane
410 localized and two not) and would presumably be trafficked via the endoplasmic reticulum to the
411 Golgi apparatus where they would be packaged into secretory vesicles for export. Further work
412 and mutagenesis of reporters may be needed to determine whether there are specific signals that
413 result in export to the PVM or PV.

414 The redirection of secretory vesicles to the PV versus to the extracellular space or cell
415 membrane in infected cells could have strong immunological consequences. A number of human
416 cytokines and proteins from the fever-causing NLRP3 inflammasome[54] including ATM, CDCA8,
417 CXCL10, CXCL2, ESPL1, H2AFX, HMOX1, LIG1, MDM2, NFKBIE, OGG1, PRIM1, PTTG1,
418 RAD50, RAD51, RELB, TDP1, TP53, TYMS, and XRCC1 are differentially regulated in late
419 infected hepatocytes via pathway analysis ($p = 0.0093$) and the redirection of secreted proteins to
420 the PV could be a mechanism to both improve parasite nutrition and evade host immune responses.
421 The antigens that would normally be displayed on the major histocompatibility complex on the
422 infected hepatocyte cell surface and present parasite antigens to T cells are now being secreted into
423 the PV space, where they cannot be recognized by CD8+ T cells.

424 Although both infected and uninfected cells were treated identically in our expression
425 dataset, the use flow sorted hepatoma cells, could create artefactual patterns. Recently a single cell
426 RNA-seq study was published[55]. Although a comprehensive comparison of the mouse and human
427 transcriptomes is outside the scope of this study, the patterns in our cell culture dual RNAseq
428 dataset are supported by single RNA-seq data from mouse liver infected with *P. berghei*. In
429 general, both datasets showed upregulation of genes involved in immune modulation and
430 decreased expression of metabolism associated genes. The single cell mouse study shows that
431 MmNR4A3 is clearly upregulated in infected mouse hepatocytes ($q = 9.18928E-06$) as is
432 MmCXCL2 ($q = 0$).

433 The reason for clinical silence of the malaria parasite infected liver cells has long been a
434 source of discussion. Bertolino and Bowen speculated that one reason CD8+ T cells poorly
435 recognize infected hepatocytes in a natural infection is because of either the low numbers of
436 infected hepatocytes, or because of natural tolerance[56]. An alternative explanation is that secretion
437 is modified in infected cells to direct products to the PV, as supported by our data. Our data may
438 also explain why irradiated sporozoites, which can complete the early stages of invasion but do
439 not progress to liver schizonts could create a better immune response. It would be interesting to
440 evaluate the distribution of organellar markers such as HsBiP, and HsGOLGA8A with irradiated
441 sporozoites.

442 How the parasite accomplishes host cell remodeling is unknown. Our data support the
443 Golgi as key to host cell remodeling. Much of the Golgi structure and function is controlled by
444 small Rab GTPases, which are key regulators of intracellular transport and membrane trafficking
445 in eukaryotic cells GTPases[57]; De Niz et al. demonstrated the functional importance of the
446 GTPases ARF1 and RAB1A, in *P. berghei* exoerythrocytic stage development, when they
447 expressed dominant negatives (with gain-of-function mutations in the nucleotide binding sites)
448 and showed that these mutants proteins caused an arrest and lower survival of the parasite in HeLa
449 cells[48]. In the related apicomplexan parasite, *T. gondii*, genetic screens have shown that the parasite
450 releases effector molecules into the host cell cytoplasm when it invades[58]. Although parasite
451 proteins that are needed for exoerythrocytic stages to develop have been identified in genome wide
452 genetic screens[59], it is not clear which of these are released into the host cell cytoplasm and which
453 are retained within the parasite. Screens of these mutants using host markers will likely be needed
454 to identify these factors.

455 One of the most interesting discoveries is that host cell remodeling is also observed in *P.*
456 *vivax* hypnozoites, as this now presents a way to disturb the PV and potentially provide a radical
457 cure. *P. vivax* hypnozoites, which presumably are not replicating their DNA and are not growing,
458 have traditionally been challenging to eliminate. The 8-aminoquinoline family of compounds that
459 can eliminate hypnozoites were discovered by injecting hundreds of macaques with random
460 compounds and testing to see which were permanently cured of malaria[60,61]. Recently, phenotypic
461 screening systems have begun to identify other types of compounds that are critical to hypnozoite
462 survival[62]. Our work shows that early-stage *P. berghei*, and *P. vivax* EEFs both redirect
463 upregulated proteins to the PVR, and this presents a way to study the process. This could
464 potentially lead to the identification of drug targets for the elusive hypnozoite.

465

466

467

468

469

470 **MATERIALS AND METHODS**

471 Note: Requests for materials should be addressed to Elizabeth A. Winzeler:
472 ewinzeler@health.ucsd.edu

473 *Parasites*

474 *P. berghei*-ANKA-GFP-Luc-SMCON (*Pb*-Luc)[63] and *P. berghei*-GFP (*Pb*-GFP)[63]
475 sporozoites were obtained by dissection of infected Anopheles stephensi[64,65] mosquito salivary
476 glands. Dissected salivary glands were homogenized in a glass tissue grinder and filtered twice
477 through nylon cell strainers (20µm pore size, Millipore SCNY00020) and counted using a
478 Neubauer hemocytometer. The sporozoites were kept on ice until needed. *Pb*-Luc and *Pb*-GFP-
479 infected *An. stephensi* mosquitoes were also obtained from the Insectary Core Facility at New
480 York University or from the Sporocore at the University of Georgia, Athens (Grant number R01
481 AI090141-08).

482 For *Pb*-Luc sporozoite production, female 6–8-week-old Swiss Webster mice (UCSD
483 Vivarium) were injected with blood stage *Pb*-Luc parasites to begin the growth cycle. Animal
484 handling was conducted according to the UCSD Institutional Animal Care and Use Committee-
485 approved protocols. *An. stephensi* mosquitoes raised at UCSD insectary were allowed to feed on
486 infected mice with gametocytemia of ~10%. Dissected thorax sporozoites were isolated using a
487 standard protocol at day 14 or 15 post-blood meal. The sporozoites were washed with DMEM
488 incomplete media to remove debris from the thorax. The sporozoites were centrifuged 15,000 × g
489 for 5 min at 4°C to pellet and resuspended in the desired volume of complete medium.

490 *P. falciparum* sporozoites strain NF54 were isolated from infected *An. stephensi* mosquito
491 salivary glands. The sporozoites were isolated at TropIQ Health Sciences. Transistorweg 5, The
492 Netheherlands.

493 *Cell culture*

494 HC-04[66], Huh7.5.1[67] and HepG2-A16-CD81^{EGFP} [68,69] cells were cultured at 37°C with 5%
495 CO_2 in complete media (DMEM (Invitrogen, Carlsbad, USA) supplemented with 10% FBS,
496 0.29mg/mL glutamine, 100 units of penicillin, and 100µg/mL streptomycin). During and after the
497 infection with *Pb*-Luc, or *Pb*-GFP, or *P. vivax* sporozoites, complete DMEM media was

498 supplemented with antibiotics 50µg/mL gentamycin, 50µg/mL neomycin, 100 units of penicillin,
499 and 100µg/mL streptomycin, also antimycotics 50µg/mL 5-fluorocytosine, 100µg/mL
500 posaconazole and 100µg/mL neomyxin.

501 Human Foreskin Fibroblast (HFF, SCRC-1041 from ATCC) were cultured in T-25 flasks
502 (Corning, #430639) at 37°C with 5% CO_2 in D10 media comprising DMEM (Thermo Fisher
503 Scientific, #12100046) supplemented with 10% FBS (GE Healthcare, #SH30071.02HI), 2mM
504 glutamine (Thermo Fisher Scientific, #25030149), 10mM HEPES (Sigma-Aldrich, #H3375),
505 44mM sodium bicarbonate (Sigma-Aldrich, #S5761), 10mg/L gentamicin (Thermo Fisher
506 Scientific, #15710072), and 100µg/mL penicillin-streptomycin. Once confluent, media is changed
507 and can be infected with *T. gondii*. Media was changed twice a week, with new monolayers made
508 every two weeks. All cell lines and source are described in Table S1.

509 *Infection of hepatocytes for qRT-PCR*

510 Hepatocytes were seeded into 24-well plates (120,000 cells per well) 24h before infection,
511 and infected with *Pb*-GFP sporozoites obtained from freshly dissected and infected *An. stephensi*
512 mosquitoes at a ratio of 0.3 sporozoites per seeded cell. Plates were centrifuged at 330 × g for 3
513 min to bring sporozoites closer to cells, and plates were then incubated at 37°C in 5% CO_2 for 2h
514 to promote sporozoite invasion[70]. After 2h, the cells were washed, fresh complete DMEM media
515 were supplemented with 12µM 5-fluorocytosine (Cayman, #11635), 50µg/mL gentamicin sulfate
516 (Gibco, #15710072), and 100µg/mL neomycin trisulfate salt hydrate (Sigma-Aldrich, #72133),
517 and the cells were returned to the incubator.

518 *Separation of infected and uninfected hepatocytes, RNA isolation and gene expression*
519 *quantification by qRT-PCR*

520 HepG2, Huh7.5.1 and HC-04 cells, in addition to primary human hepatocytes, were
521 dissociated from plates at time zero (uninfected hepatocytes and sporozoites before infection), 24
522 and 48hpi by the addition of 500µL TrypLE Express (1×, ThermoFisher, #12605010), washed
523 once using 1× PBS (Gibco, #14190144) and resuspended in FACS buffer (1× PBS supplemented
524 with 1mM EDTA, 25mM HEPES and 0.5%FBS), then passed through a 40µm cell strainer prior
525 to sorting (BD Falcon). Uninfected and infected cells were isolated by FACS using a BD Influx
526 cell sorter with GFP mean fluorescence intensity (MFI) used to determine infection status. Overall

527 gating strategy is as previously reported[17], and shown in Fig. S12 with total cells identified via
528 Forward Scatter (FSC) vs Side Scatter (SSC) (P1 gate), individual cells identified via tandem
529 gating of FSC-Height vs FSC-width and SSC-Height vs SSC-Width (gates P2 and P3), then GFP
530 positive and negative cells were collected as indicated (gates P4, and P5 respectively). For RNA
531 extraction, cells were directly sorted into Eppendorf tubes containing 600µL Qiazol reagent
532 (Qiagen) and total RNA was extracted using the Qiagen miRNEasy Mini kit (Qiagen, #217004)
533 according to manufacturer's instructions. Gene expression differences were measured using SYBR
534 green qRT-PCR with PerfeCTa SYBR® Green FastMix (Quanta Bio, #95054), using the primers
535 indicated in Table S2, and a Bio-Rad CFX96 qRT-PCR system (Bio-Rad). Changes were
536 quantitated according to the ΔΔCT method and normalized using Human Beta-2-Microglobulin
537 (*B2M*) gene.

538 *Dual RNA-sequencing analysis and code availability*

539 We analyzed the gene differential expression using data previously generated and obtained
540 in our group[17]. Reads can be found in the short read archive (http://www.ncbi.nlm.nih.gov/sra),
541 under accession number PRJNA390648. We took the dual RNA-seq read count tables from the
542 same study, and used DESeq2[71] with a multifactorial design, to calculate gene differential
543 expression at both 24 and 48h for infected versus uninfected cells, in HepG2s, Huh7.5.1s and HC-
544 04s cell lines as well as using HC-04 cells alone.

545 *Determination of infection in hepatocytes through RNA quantification by qRT-PCR*

546 Quantification of *Pb*-Luc infection was as previously described[72]. Briefly, 90,000 HC-04
547 HsNR4A3 WT and CRISPR/*Cas*9 edited cells were plated 24h before infection in 24-well plates.
548 *Pb*-Luc parasites were added at a 1:2 ratio and complete DMEM media was changed 2h later.
549 After 48h, infected cells were harvested and washed gently with PBS. RNA was isolated using
550 Qiagen miRNEasy Mini Kit (Qiagen, #217004) according to manufacture instructions. RNA was
551 quantified using a Nanodrop (Thermo Scientific) and cDNAs were synthetized using
552 SuperScript™ II Reverse Transcriptase kit (Invitrogen, #18064022). Gene expression levels for
553 parasite 18S RNA were then assessed by SYBR green qRT-PCR using perfecta SYBR Green
554 FastMix (Applied Biosystems, #4367659), the set of primers described in Table S2, a Bio-Rad

555 CFX realtime PCR system and quantitated using the ΔCT method and normalized against Human
556 Hypoxanthine phosphoribosyltransferase 1 (*HPRT1*) gene.

557 *Western blot of CRISPR/Cas9 edited cell lines*

558 Cells were first plated, infected, and sorted for GFP as described above. After sorting,
559 1,000 infected or 150,000 uninfected cells were washed twice with cold 1× PBS. Cells were lysed
560 via the addition of 200µL RIPA buffer (Teknova, #R3792) plus 1:100 protease inhibitor (Halt –
561 Thermo Fisher Scientific, #78429). Equal numbers of cells were loaded onto the gel in 2× Laemmli
562 Buffer (BioRad, #1610737), and proteins were loaded onto 18-well BioRad anyKD Criterion TGX
563 gels (Bio-Rad, #5671124). For validation of HsNR4A3 protein knockout, 10µg of protein from
564 uninfected HC-04 WT and CRISPR/*Cas*9 edited cell lines were lysed in RIPA buffer as above and
565 loaded into identical gels.

566 Approach 1: Proteins were transferred to membranes and were probed with primary α-
567 HsNR4A3 (dilution 1:100; #ab56340), and α-HsVinculin (dilution 1:100; #ab129002) antibodies
568 overnight at 4°C, probed with goat α-rabbit HRP secondary (dilution 1:5,000; #G21234), and
569 detected using Super Signal West Pico, and Femto Chemiluminescent Substrate (Thermo Fisher,
570 #34577 and #34090). Densitometry was calculated using ImageJ (http://rsbweb.nih.gov/ij/) after
571 image inversion and is shown relative to loading control.

572 Approach 2: Proteins were transferred to membranes and were probed with primary α-
573 HsNR4A3 (dilution 1:100; #TA804893), and α-HsVinculin (dilution 1:100; #4650S) antibodies
574 overnight at 4°C, probed with goat α-mouse HRP secondary (dilution 1:5,000; #7076P2) or goat
575 α-rabbit HRP secondary (dilution 1:5,000; #7074S), and detected using SuperSignal West Pico
576 and Femto Chemiluminescent Substrate (Thermo Fisher, #34577 and #34095), images were
577 acquired using a gel documentation and analysis system (Syngene, G:Box) and the software Gen
578 Sys V.1.4.3.0. Densitometry was calculated using ImageJ (http://rsbweb.nih.gov/ij/) after image
579 inversion and is shown relative to loading control.

580 *Plasmodium exoerythrocytic form (EEF) culture for cellular localization*

581 For *Pb*-Luc imaging, 96-well glass bottom plates (MatTek Corporation) or 8-well Nunc
582 Lab-Tek slides (Thermo Scientific, #125658) were coated with Poly-L-Lysine 0.01% (v/v)
583 (Sigma, #P4707) and subsequently seeded with HC-04 cells (2,500 or 25,000 cells per well,

584 respectively) 24h before infection. *Pb*-Luc sporozoites were freshly isolated from infected *An.*
585 *stephensi* mosquitoes as above and resuspended in screening DMEM media (DMEM media
586 supplemented with 5% FBS, 1.46mg/mL glutamine, 500 units of penicillin, and 500µg/mL
587 streptomycin), and additionally we added 0.5µM posaconazole (Cayman), 12µM 5-fluorocytosine
588 (Cayman), 50µg/mL gentamicin sulfate (Gemini Bio-Products), and 100µg/mL neomycin
589 trisulfate salt hydrate (Sigma-Aldrich). Pre-seeded well plates were infected with *Pb*-Luc
590 sporozoites using a 1:2 infection ratio (sporozoite to cell) and incubated for 2h at 37°C in 5% CO_2.
591 After 2h infection, medium was replaced, and plates were incubated for 48h.

592 *P. falciparum experiments*

593 Sixty thousand human primary hepatocytes were seeded in 60 wells of a collagen-coated
594 96 well microtiter plate. Two days after seeding, cells were infected with fifty thousand sporozoites
595 of *Plasmodium falciparum* strain NF54 (isolated from infected *An. Stephensi* mosquitos). Five
596 days post-infection, cells were fixed with methanol, permeabilized, blocked, incubated with
597 different primary antibodies, and evaluated by immunofluorescence and confocal microscopy.

598 *P. vivax experiments*

599 *P. vivax* sporozoites were isolated from infected *An. darlingi* mosquitoes from a laboratory-
600 established colony in the Peruvian Amazon region[73,74]. Briefly, 30 patients (18 years and older)
601 from the Iquitos region, who were diagnosed with *P. vivax* malaria by blood smear and who had
602 not received treatment yet were enrolled. Approximately 20mL of whole blood was collected.
603 After centrifugation at 500 × *g* for 5 min at 37°C, plasma was removed from the *P. vivax*-infected
604 packed red cells and replaced with an equal volume of heat inactivated O^+ plasma. Then the red
605 cells were used to feed fasted female *An. darlingi* mosquitoes using a standard membrane feeding
606 assay as previously described[73,74]. After seven days, a group of ten mosquitos were midgut
607 dissected and stained by mercurochrome to evaluate oocyst development, and 14 days after the
608 first infection mosquitoes were dissected to obtain sporozoites. Dissected salivary glands were
609 homogenized in a 1.5mL tube, crushed with a homogenizer, filtered twice using nylon cell strainers
610 (20µm pore size, Millipore SCNY00020), centrifuged, and resuspended in a 500µL final volume.
611 The number of sporozoites were counted using Neubauer hematocytometer. The sporozoites were
612 kept on ice until needed.

613 For Western blot assays, 6-well glass bottom plates (Thermo Scientific, #NUNC-140675)
614 were coated with Poly-L-Lysine 0.01% (v/v) (Sigma, #P4707) and seeded with HC-04 WT cells
615 (800,000 cells per well) 24h before *P. berghei* or *P. falciparum* NF54 sporozoites infection
616 (400,000 sporozoites per well). *P. berghei* or *P. falciparum* NF54 were diluted in DMEM media
617 using 1:2 infection ratio (sporozoites to HC-04 cells) and incubated 4h at 37°C under 5%CO_2
618 atmosphere. After this initial incubation period, infection media was replaced with fresh screening
619 DMEM media, plates with HC-04 cells infected with *P. berghei* were incubated for two days, and
620 the plates with HC-04 cells infected with *P. falciparum* were incubated for five days, the screening
621 DMEM media was replaced every 24h.

622 Uninfected and infected cells were lysed via the addition of 200µL RIPA buffer (Fisher
623 Scientific, #P189900) plus protease inhibitor cocktail (cOmplete Mini, EDTA-free – Roche,
624 #11836170001). Proteins (50µg) were mixed with 2× Laemmli Buffer (BioRad, #1610737), and
625 loaded onto 12-well BioRad Criterion TGX gels (Bio-Rad, #5671083). Proteins were transferred
626 to nitrocellulose membranes and were different primary antibodies overnight at 4°C (Table S2),
627 probed with goat α-mouse HRP secondary antibody (dilution 1:2,000; #7076P2), goat α-rabbit
628 HRP secondary antibody (dilution 1:2,000; #7074S) or rabbit α-goat HRP secondary antibody
629 (dilution 1:2,000; #A27014), and detected using SuperSignal West Pico or Femto
630 Chemiluminescent Substrate (Thermo Fisher, #34577 and #34095), images were acquired using a
631 gel documentation and analysis system (Syngene, G:Box) and the software Gen Sys V.1.4.3.0.

632 For IFA analysis 96-well glass bottom plates (MatTek Corporation) or 8-well Nunc Lab-
633 Tek chamber slides (Thermo Scientific, #125658) were coated with Poly-L-Lysine 0.01% (v/v)
634 (Sigma, #P4707) and seeded with HC-04 WT or CRISPR/*Cas*9 edited cells (2,500 or 25,000 cells
635 per well) 24h prior to mosquito dissection and infection. *P. vivax* sporozoites were diluted in
636 screening DMEM media (supplemented as above). Slides were infected using a 1:2 infection ratio
637 (sporozoites to HC-04 cells) and incubated for 4h at 37°C under 5%CO_2 atmosphere. After this
638 initial incubation period, infection media was replaced with fresh screening DMEM media, and
639 plates or slides were incubated for five days, the screening DMEM media was replaced every 24h.

640 *Plasmodium EEF and HsNR4A3 immunofluorescence microscopy and high content imaging*

641 All primary and secondary antibodies used in this study are given in Table S3-S5. For
642 HsNR4A3 antibody #1 (dilution 1:100; #TA84893) or #2 (dilution 1:100; #Ab56340), we used
643 HC-04 HsNR4A3 wild type, CRISPR/*Cas*9 edited cells lines and the *Pb*-Luc parasites[75]. We
644 seeded the cells in 8-well chamber slides and infected them with a 1:2 infection ratio (sporozoite
645 to HC-04 cell). After 48h of infection, cells were fixed with 4% paraformaldehyde-PBS
646 (Affymetrix, #19943) for 20 min at RT, permeabilized with 0.1% TritonX-100 (Fisher,
647 #BP151500) for 10 min at RT, blocked with 1% BSA for 1h and incubated with two antibodies
648 overnight at 4°C. The first antibody was a PbUIS4 (*P. berghei* UIS4) goat polyclonal antibody
649 (dilution 1:500; #LS-C204260), the second antibody was HsNR4A3 mouse monoclonal antibody
650 (dilution 1:100; #TA804893). Then, the following secondary antibodies were used 1) Donkey α-
651 Goat Alexa Fluor 488 (dilution 1:1,000; #705-546-147) and Goat α-Mouse Rhodamine Red™-X
652 (#115-295-071) or Rhodamine Red™-X (1:1,000; #805-297-008) for 2h at RT. Hepatocyte plasma
653 membrane was detected using CellMask deep red (Thermo Fisher Scientific, #C10046) at 1×.
654 After IFA, chambers were removed from *Pb*-Luc-infected Lab-Tek systems, slides were mounted
655 with Vectashield with DAPI (Vector Labs, #H-1500) and #1.5 glass coverslips were affixed using
656 nail polish. Images were acquired using a Zeiss LSM880 with Airyscan Confocal Microscope (63×
657 Plan-Apochromat /1.4 NA DIC oil immersion objective); laser power was set to 3% for 405, 488,
658 561, and 640nm. The images were processed using the confocal ZEN software (Black edition,
659 Zeiss). The level of colocalization between the two fluorescent proteins (α-PvUIS4/α-HsNR4A3,
660 α-PvUIS4/α-HsCGA, α-PvUIS4/α-HsGOLGA8A, α-PvUIS4/α-HsMUC13, or α-PvUIS4/α-
661 HsCXCL2 were determined by calculating the product of the difference from the mean (PDM)
662 indicated a mean Pearson coefficient r (Pearson correlation coefficient - PCC) in PV, α-PvUIS4
663 was on channel A vs human host protein on Channel B. The PCC were analyzed using Volocity
664 3D/4D rendering software for three identified objects from each of three biological replicates.

665 *Ultrastructure Expansion Microscopy (U-ExM)*

666 Clean coverslips (Fisher Scientific, #NC1129240) pretreated with poly-l-lysine for 1h at
667 37°C, washed with MilliQ water, dried, and placed in the wells of a 12-well plate, were used to
668 seed human liver cells (HC-04 or Huh7.5.1 cells, 200,000) resuspended in 1ml of DMEM complete

669 media and incubated at 37°C, 5% $C0_2$, for 24h. The infection was performed with *P. berghei*
670 sporozoites (100,000) at ratio 2:1 (two cells to one parasite), incubated during 48h, 37°C, 5% $C0_2$.
671 Supernatants were removed, and the cells were fixed with 1 mL of 4% PFA (EMS #15710)/PBS
672 for 20 min at 37°C. then stored and shipped overnight to the Absalon lab at Indiana University
673 School of Medicine. At reception, coverslips were proceeded for expansion microscopy as
674 described in Liffner and Absalon 2021[38]. Gels were incubated overnight with primary antibodies
675 with the following dilution 1:250 for α-PvUIS4 and 1:100 for α-HsNR4A3 at room temperature
676 on a shaker. All secondary antibodies were diluted 1:500 in PBS (Donkey anti-Goat-Alexa488,
677 ThermoFisher Scientific #A-11055 and Donkey anti-Mouse-Alexa555, ThermoFisher Scientific
678 #A-31570), 1:250 for NHS ester-Alexa405 (ThermoFisher Scientific #A7573) and 1:1000 for
679 Sytox™ Deep red (ThermoFisher Scientific #S11380) and incubated room temperature on a shaker
680 for 2h and 30 min. Staining with 1:1000 Bodipy-TR-Ceramide (ThermoFisher Scientific #D7540)
681 required an additional overnight room temperature on a shaker.

682 For imaging, small sections of the larger gel were cut and gently dried before being placed
683 into 35 mm #1.5 coverslips bottomed imaging dishes (Cellvis; Fisher Scientific #NC0409658)
684 precoated with poly-D-lysine. The images were acquired using a Zeiss LSM900 AxioObserver
685 microscope with Airyscan 2 detector, with 63x Plan-Apochromat (NA 1.4) objective lens. All
686 images were acquired in multiplex mode 2 as Z-stacks with and XY pixel size 0.035 µm and a Z-
687 step size of 0.13 µm, and processed using Zen Blue software (Version 3.5, Zeiss, Oberkochen,
688 Germany).

689 *High content imaging (HCI) of edited lines*

690 HC-04[66] CRISPR/*Cas*9 edited cell lines were seeded in 384-well plates or 8-well Lab-Tek
691 slides and infected with *Pb*-Luc parasites[63] at a ratio 2:1 (cells/sporozoites). After 48h cells were
692 fixed, permeabilized, blocked and incubated with PbUIS4 polyclonal antibody (dilution 1:500;
693 #LS-C204260) and HsNR4A3 monoclonal antibody (dilution 1:100; #TA804893). The data were
694 acquired (image analysis) using a High Content Imaging System (Operetta®, PerkingElmer).
695 Nuclei (DAPI) were detected using an excitation wavelength of 360-400nm, emission 410-480nm,
696 with exposure time at 200 milliseconds (ms), and a height 40µm. PbUIS4 protein was detected
697 using the Alexa 488 channel (excitation 460-490, emission 500-550nm), exposure time of 200ms,

698 and height of 82µm. HsNR4A3 protein was detected using the Alexa 568 channel (excitation 560-
699 580, emission 590-640nm) with exposure time 200ms and height 82µm. Plasma membranes were
700 detected using the DRAQ5 channel (excitation 620-640nm, emission 650-760nm) with exposure
701 time of 200ms and a height 80µm.

702 To evaluate and determined the size of *P. berghei* schizonts forms we use a splitting
703 coefficient of 0.40; common threshold, 0.40, split factor 72.0; individual threshold, 0.50; contrast,
704 0.50. Schizonts were also evaluated using different sets for diameter: 5, 20, 30 and 40µm^2. The
705 images were captured using a 10× long WD/0.3 NA objective, 10× magnification, 10 fields, 1
706 plane and 1 time point.

707 *Cytokine HsCXCL2 stimulation with lipopolysaccharide (LPS)*

708 To evaluate the expression of human chemokine HsCXCL2 (GROß), *in vitro* infections
709 were performed using the human liver line HC-04 with *P. berghei* sporozoites, or HFF1 cells and
710 *T. gondii* parasites in 8-well Lab-Tek slides. Cells were stimulated by treatment with 1µg/mL
711 lipopolysaccharide (LPS), from *E. coli* O55: B5 (Sigma Aldrich, # L6529). Cells were treated
712 with LPS at 24hpi and collected for confocal microscopy at 24, and 48h. The expression and
713 localization of HsCXCL2 protein in HC-04 cells and HFF cells were visualized through the use of
714 the anti-HsCXCL2 primary antibody (dilution 1:100; Table S3). *P. berghei* parasites were
715 visualized α-PbUIS4 polyclonal antibody (dilution 1:500; #LS-C204260), and *T. gondii* parasites
716 with α-*T. gondii* P30/3 (dilution 1:100; Table S3) and their respective secondary antibodies.
717 Plasma membranes were detected using CellMask deep red, and nucleus were stained with DAPI.

718 *HsNR4A3 CRISPR/Cas9 (Approach 1)*

719 HsNR4A3 was edited using a sequential two plasmid CRISPR/*Cas9* approach. First, HC-
720 04 cells expressing CAS9 were generated using lentivirus containing the EF1a-*Cas9*-2A-
721 Blasticidin Lenti plasmid (Sigma Aldrich, #LVCAS9BST-1EA). HC-04 cells were plated at a
722 density of 120,000 cells per well in three independent wells of a 24 well plate. Twenty-four hours
723 after plating, media was replaced with complete media (as above) plus 5µg/mL polybrene and viral
724 particles. Cas9 lentiviral particles were added at a multiplicity of infection (MOI) of 0.5, after
725 which cells were spun at 800 × g for 30 min, then incubated overnight at 37°C. The following day
726 media, was changed to complete media and cells were again incubated overnight at 37°C. The

727 next day, cells were selected for presence of the CAS9 plasmid using complete media plus
728 2.5µg/mL blasticidin (Thermo Fisher, #A1113903). After 14 days of selection, splitting as
729 required, cells were trypsinized and plated at an average density of one cell per well in a 96 well
730 plate in complete media plus blasticidin as above. Once cells had regrown, wells were observed
731 via microscopy to identify those wells which appeared to contain single colonies. CAS9
732 expression within clones was then confirmed via PCR.

733 Once CAS9 expressing HC-04 cells were established, gRNA targeting *HsNR4A3* was
734 introduced via Lentivirus containing the LV04 U6-gRNA:hPGK-Puro-2A-BFP plasmid and a
735 gRNA sequence specific for Human *HsNR4A3*. The DNA sequence targeted by the gRNA for
736 *HsNR4A3* was CTGCAGCAGCCTGGTCAGTGGG (Sigma-Aldrich Sanger Clone ID
737 HS5000010424). Cells were infected with virus and cultured overnight as above. The following
738 day, cells were selected for presence of the gRNA plasmid using complete media plus 2.5µg/mL
739 puromycin (Gibco, #A1113803) and 2.5µg/mL blasticidin. Clonal cell lines expressing the gRNA
740 and CAS9 were generated as previously stated. The presence of *HsNR4A3* knockout within these
741 apparent monoclonal HC-04 cell lines was examined at the protein level, after being expanded into
742 25cm^2 vented tissue culture flasks, via western blot using the HsNR4A3 rabbit polyclonal antibody
743 (dilution 1:100; Abcam, #ab56340). Three edited clones (clones GL1, GL2, and GL3) were then
744 examined using confocal microscopy, all exhibited low or no host cell HsNR4A3 protein
745 expression.

746 *HsNR4A3 CRISPR/Cas9 (Approach 2)*

747 A second round of editing for *HsNR4A3* was performed using a single plasmid
748 CRISPR/*Cas9* system with the Edit-R All-in-one Lentiviral an sgRNA, targeting *HsNR4A3*,
749 packaged in a lentiviral vector (Horizon, Perkin Elmer). The gRNA sequence used was
750 TTCGACGTCTCTTGTCTACT, targeting exon 5 of *HsNR4A3* coding sequence. Briefly, HC-04
751 cells were plated at a density of 150,000 cells per well in a 6 well plate, then 24h later media was
752 replaced with complete media supplemented with 10µg/mL polybrene. Virus was added at a
753 multiplicity of infection of one and then incubated overnight at 37°C. After 48h, the cells were
754 selected for presence of the CAS9 plasmid using complete media plus 2.5µg/mL puromycin. After
755 seven days of selection, cells were trypsinized and plated at an average density of 0.5 cell per well

756 in a 96-well plate in the presence of 2.5µg/mL puromycin for clonal selection. After ~15-20 days,
757 wells were observed via microscopy to identify those wells which contained single colonies. These
758 cells were then transferred to 6-well plates and the knockout of HsNR4A3 was confirmed in these
759 apparent monoclonal HC-04 cell lines with immunoblotting.

760 Since, in the above obtained clones, there was only partial knockout of HsNR4A3, another
761 round of transductions was performed using guide RNA GCTCGAGTAGCCCTCCACGA
762 targeting at exon 4. Lenti-V2-Blast (lentiCRISPR v2-Blast plasmid, Addgene) plasmid was used
763 here. Transductions were performed, as mentioned above, and the transformed cells were selected
764 using 1µg/mL blasticidin and 2.5µg/mL puromycin. The clones obtained after clonal selection
765 were evaluated for HsNR4A3 expression by immunoblotting using the HsNR4A3 mouse
766 monoclonal antibody (dilution 1:100; #TA804893). Three knockdown clones (clones NM1, NM2,
767 and NM3) were selected to have low HsNR4A3 expression. These clones were then used for
768 further studies.

769 ETHICS STATEMENT

770 Human subject protocols were approved by the Human Research Protection Program of
771 the University of California, San Diego (approval number 120652) and Universidad Peruana
772 Cayetano Heredia (approval number 102357). Written informed consent was obtained from all
773 study participants.

774 ACKNOWLEDGMENTS

775 We thank the members of the Winzeler laboratory for advice and critical reading of the
776 manuscript. In addition, we thank Medicines for Malaria Venture and Fogarty International Center
777 of the National Institutes of Health (NIH) under Award Number D43TW009343 and the University
778 of California Global Health Institute (UCGHI) for all their support of the insectary in Peru. We
779 would also like to thank the UCSD Human Embryonic Stem Cell Flow Cytometry Core Facility,
780 and UCSD Microscopy Core – NINDS NS047101 for their technical support. JC was supported
781 by the Fogarty International Center of the National Institutes of Health (NIH) under Award
782 Number D43TW009343 and the University of California Global Health Institute (UCGHI). GL

783 was supported by an A.P. Giannini Post-Doctoral Fellowship. EAW is supported by grants from
784 the NIH (1R01AI152533 and R01AI103058), and MMV. The *P. vivax* work was supported by
785 grants to JMV from the NIH (D43TW007120 and U19AI089681) and MMV. GTW was supported
786 by NIH training grant T32AI007036. M.R. lab funded by the NIH grants AI126277, AI145325,
787 AI154644, AI114625, by the Chiba University-University of California-San Diego (UCSD)
788 Center for Mucosal Immunology, Allergy, and Vaccines, and by the UCSD Department of
789 Pediatrics. M.R. also holds an Investigator in the Pathogenesis of Infectious Disease Award from
790 the Burroughs Wellcome Fund.

791

792 **AUTHOR CONTRIBUTIONS**

793 JC performed Immunofluorescence, HCI, qRT-PCR, Western blot assays and data
794 analysis. GL infected and sorted liver cells, isolated RNA for both infected and uninfected
795 populations and measured gene expression levels via qRT-PCR and Western blot. JC and LG
796 performed *P. vivax* liver stage assays. GL, BYZ, EP and NM generated *HsNR4A3* edited cell lines.
797 JC, GL and EW wrote the manuscript. KPGM analyzed data and created figures. BC contributed
798 concepts and helped fund the study. KC performed *T. gondii* infections. CTR, DG and JV
799 developed methods and infrastructure for *P. vivax* infections. GTW performed ELISA assays for
800 HsCXCL2 protein. SA and BL performed U-ExM and imaging. All authors assisted with editing
801 of the manuscript. The authors declare no conflicts of interest or competing financial interests.

802

803

804

805

806

807

808

809 **REFERENCES**

810 1 Fodor, S. P. *et al.* Multiplexed biochemical assays with biological chips. *Nature* **364**, 555-
811 556 (1993).

812 2 Pradel, G. & Frevert, U. Malaria sporozoites actively enter and pass through rat Kupffer
813 cells prior to hepatocyte invasion. *Hepatology* **33**, 1154-1165 (2001).
814 https://doi.org:10.1053/jhep.2001.24237

815 3 Barnwell, J. W. Hepatic Kupffer cells: the portal that permits infection of hepatocytes by
816 malarial sporozoites? *Hepatology* **33**, 1331-1333 (2001).
817 https://doi.org:10.1053/jhep.2001.24740

818 4 Frischknecht, F. & Matuschewski, K. Plasmodium Sporozoite Biology. *Cold Spring Harb*
819 *Perspect Med* **7** (2017). https://doi.org:10.1101/cshperspect.a025478

820 5 Mota, M. M., Hafalla, J. C. & Rodriguez, A. Migration through host cells activates
821 Plasmodium sporozoites for infection. *Nat Med* **8**, 1318-1322 (2002).
822 https://doi.org:10.1038/nm785

823 6 Sinai, A. *The Toxoplasma gondii Parasitophorous Vacuole Membrane: A multifunctional*
824 *Organelle in the Infected Cell*. (2014).

825 7 Markus, M. B. Malaria: origin of the term "hypnozoite". *J Hist Biol* **44**, 781-786 (2011).
826 https://doi.org:10.1007/s10739-010-9239-3

827 8 Vaughan, A. M. & Kappe, S. H. I. Malaria Parasite Liver Infection and Exoerythrocytic
828 Biology. *Cold Spring Harb Perspect Med* **7** (2017).
829 https://doi.org:10.1101/cshperspect.a025486

830 9 Wilby, K. J., Lau, T. T., Gilchrist, S. E. & Ensom, M. H. Mosquirix (RTS,S): a novel
831 vaccine for the prevention of Plasmodium falciparum malaria. *Ann Pharmacother* **46**, 384-
832 393 (2012). https://doi.org:10.1345/aph.1AQ634

833 10 Casares, S., Brumeanu, T. D. & Richie, T. L. The RTS,S malaria vaccine. *Vaccine* **28**,
834 4880-4894 (2010). https://doi.org:10.1016/j.vaccine.2010.05.033

835 11 Laurens, M. B. RTS,S/AS01 vaccine (Mosquirix?): an overview. *Human Vaccines &*
836 *Immunotherapeutics* **16**, 480-489 (2020). https://doi.org:10.1080/21645515.2019.1669415

837 12 Nussenzweig, R., Vanderberg, J. & Most, H. Protective immunity produced by the
838 injection of x-irradiated sporozoites of Plasmodium berghei. IV. Dose response, specificity
839 and humoral immunity. *Mil Med* **134**, 1176-1182 (1969).

840 13 Sharma, S. & Pathak, S. Malaria vaccine: a current perspective. *J Vector Borne Dis* **45**, 1-
841 20 (2008).

842 14 Goh, Y. S., McGuire, D. & Renia, L. Vaccination With Sporozoites: Models and Correlates
843 of Protection. *Front Immunol* **10**, 1227 (2019). https://doi.org:10.3389/fimmu.2019.01227

844 15 Leiriao, P., Mota, M. M. & Rodriguez, A. Apoptotic Plasmodium-infected hepatocytes
845 provide antigens to liver dendritic cells. *J Infect Dis* **191**, 1576-1581 (2005).
846 https://doi.org:10.1086/429635

847 16 Vaughan, A. M., Wang, R. & Kappe, S. H. Genetically engineered, attenuated whole-cell
848 vaccine approaches for malaria. *Hum Vaccin* **6**, 107-113 (2010).
849 https://doi.org:10.4161/hv.6.1.9654

850 17 LaMonte, G. M. *et al.* Dual RNA-seq identifies human mucosal immunity protein Mucin-
851 13 as a hallmark of Plasmodium exoerythrocytic infection. *Nat Commun* **10**, 488 (2019).
852 https://doi.org:10.1038/s41467-019-08349-0

853 18 Mueller, A. K. *et al.* Plasmodium liver stage developmental arrest by depletion of a protein
854 at the parasite-host interface. *Proc Natl Acad Sci U S A* **102**, 3022-3027 (2005).
855 https://doi.org:10.1073/pnas.0408442102

856 19 Bertiaux, E. *et al.* Expansion microscopy provides new insights into the cytoskeleton of
857 malaria parasites including the conservation of a conoid. *PLoS Biol* **19**, e3001020 (2021).
858 https://doi.org:10.1371/journal.pbio.3001020

859 20 McGuckin, M. A., Linden, S. K., Sutton, P. & Florin, T. H. Mucin dynamics and enteric
860 pathogens. *Nat Rev Microbiol* **9**, 265-278 (2011). https://doi.org:10.1038/nrmicro2538

861 21 Fu, Y., Luo, L., Luo, N., Zhu, X. & Garvey, W. T. NR4A orphan nuclear receptors
862 modulate insulin action and the glucose transport system: potential role in insulin
863 resistance. *J Biol Chem* **282**, 31525-31533 (2007).
864 https://doi.org:10.1074/jbc.M701132200

865 22 Reynolds, M. S. *et al.* beta-Cell deletion of Nr4a1 and Nr4a3 nuclear receptors impedes
866 mitochondrial respiration and insulin secretion. *Am J Physiol Endocrinol Metab* **311**, E186-
867 201 (2016). https://doi.org:10.1152/ajpendo.00022.2016

868 23 Close, A. F., Dadheech, N., Villela, B. S., Rouillard, C. & Buteau, J. The orphan nuclear
869 receptor Nor1/Nr4a3 is a negative regulator of beta-cell mass. *J Biol Chem* **294**, 4889-4897
870 (2019). https://doi.org:10.1074/jbc.RA118.005135

871 24 Duez, H. & Pourcet, B. Nuclear Receptors in the Control of the NLRP3 Inflammasome
872 Pathway. *Front Endocrinol (Lausanne)* **12**, 630536 (2021).
873 https://doi.org:10.3389/fendo.2021.630536

874 25 Fedorova, O. *et al.* Orphan receptor NR4A3 is a novel target of p53 that contributes to
875 apoptosis. *Oncogene* **38**, 2108-2122 (2019). https://doi.org:10.1038/s41388-018-0566-8

876 26 Casarini, L., Santi, D., Brigante, G. & Simoni, M. Two Hormones for One Receptor:
877 Evolution, Biochemistry, Actions, and Pathophysiology of LH and hCG. *Endocr Rev* **39**,
878 549-592 (2018). https://doi.org:10.1210/er.2018-00065

879 27 Bieche, I. *et al.* The CGA gene as new predictor of the response to endocrine therapy in
880 ER alpha-positive postmenopausal breast cancer patients. *Oncogene* **20**, 6955-6959 (2001).
881 https://doi.org:10.1038/sj.onc.1204739

882 28 Lu, P., Zhang, C. H., Lifshitz, L. M. & ZhuGe, R. Extraoral bitter taste receptors in health
883 and disease. *J Gen Physiol* **149**, 181-197 (2017). https://doi.org:10.1085/jgp.201611637

884 29 Zhang, P., Cao, L., Zhou, R., Yang, X. & Wu, M. The lncRNA Neat1 promotes activation
885 of inflammasomes in macrophages. *Nat Commun* **10**, 1495 (2019).
886 https://doi.org:10.1038/s41467-019-09482-6

887 30 Kim, J. *et al.* Long noncoding RNA MALAT1 suppresses breast cancer metastasis. *Nat*
888 *Genet* **50**, 1705-1715 (2018). https://doi.org:10.1038/s41588-018-0252-3

889 31 Menon, M. P. & Hua, K. F. The Long Non-coding RNAs: Paramount Regulators of the
890 NLRP3 Inflammasome. *Front Immunol* **11**, 569524 (2020).
891 https://doi.org:10.3389/fimmu.2020.569524

892 32 Liu, J. *et al.* The role of the Golgi apparatus in disease (Review). *Int J Mol Med* **47** (2021).
893 https://doi.org:10.3892/ijmm.2021.4871

894 33 Gillingham, A. K. & Munro, S. Finding the Golgi: Golgin Coiled-Coil Proteins Show the
895 Way. *Trends Cell Biol* **26**, 399-408 (2016). https://doi.org:10.1016/j.tcb.2016.02.005

896 34 Mikolajczak, S. A. *et al.* Plasmodium vivax liver stage development and hypnozoite
897 persistence in human liver-chimeric mice. *Cell Host Microbe* **17**, 526-535 (2015).
898 https://doi.org:10.1016/j.chom.2015.02.011

899 35 Nomiyama, T. *et al.* The NR4A orphan nuclear receptor NOR1 is induced by platelet-
900 derived growth factor and mediates vascular smooth muscle cell proliferation. *J Biol Chem*
901 **281**, 33467-33476 (2006). https://doi.org:10.1074/jbc.M603436200

902 36 Jakymiw, A. *et al.* Identification and characterization of a novel Golgi protein, golgin-67.
903 *J Biol Chem* **275**, 4137-4144 (2000). https://doi.org:10.1074/jbc.275.6.4137

904 37 Friesen, J. *et al.* Natural immunization against malaria: causal prophylaxis with antibiotics.
905 *Sci Transl Med* **2**, 40ra49 (2010). https://doi.org:2/40/40ra49 [pii]

906 10.1126/scitranslmed.3001058

907 38 Liffner, B. & Absalon, S. Expansion Microscopy Reveals Plasmodium falciparum Blood-
908 Stage Parasites Undergo Anaphase with A Chromatin Bridge in the Absence of Mini-

Chromosome Maintenance Complex Binding Protein. *Microorganisms* **9** (2021). https://doi.org:10.3390/microorganisms9112306

39 De Filippo, K. *et al.* Mast cell and macrophage chemokines CXCL1/CXCL2 control the early stage of neutrophil recruitment during tissue inflammation. *Blood* **121**, 4930-4937 (2013). https://doi.org:10.1182/blood-2013-02-486217

40 Posfai, D. *et al.* Plasmodium parasite exploits host aquaporin-3 during liver stage malaria infection. *PLoS Pathog* **14**, e1007057 (2018). https://doi.org:10.1371/journal.ppat.1007057

41 Agop-Nersesian, C. *et al.* Shedding of host autophagic proteins from the parasitophorous vacuolar membrane of Plasmodium berghei. *Sci Rep* **7**, 2191 (2017). https://doi.org:10.1038/s41598-017-02156-7

42 Grutzke, J. *et al.* The spatiotemporal dynamics and membranous features of the Plasmodium liver stage tubovesicular network. *Traffic* **15**, 362-382 (2014). https://doi.org:10.1111/tra.12151

43 Real, E. *et al.* Plasmodium UIS3 sequesters host LC3 to avoid elimination by autophagy in hepatocytes. *Nat Microbiol* **3**, 17-25 (2018). https://doi.org:10.1038/s41564-017-0054-x

44 Schmuckli-Maurer, J. *et al.* Inverted recruitment of autophagy proteins to the Plasmodium berghei parasitophorous vacuole membrane. *PLoS One* **12**, e0183797 (2017). https://doi.org:10.1371/journal.pone.0183797

45 Niklaus, L. *et al.* Deciphering host lysosome-mediated elimination of Plasmodium berghei liver stage parasites. *Sci Rep* **9**, 7967 (2019). https://doi.org:10.1038/s41598-019-44449-z

46 Agop-Nersesian, C., Niklaus, L., Wacker, R. & Theo Heussler, V. Host cell cytosolic immune response during Plasmodium liver stage development. *FEMS Microbiol Rev* **42**, 324-334 (2018). https://doi.org:10.1093/femsre/fuy007

47 Bano, N., Romano, J. D., Jayabalasingham, B. & Coppens, I. Cellular interactions of Plasmodium liver stage with its host mammalian cell. *Int J Parasitol* **37**, 1329-1341 (2007). https://doi.org:10.1016/j.ijpara.2007.04.005

48 De Niz, M. *et al.* Hijacking of the host cell Golgi by Plasmodium berghei liver stage parasites. *J Cell Sci* **134** (2021). https://doi.org:10.1242/jcs.252213

49 Deschermeier, C. *et al.* Mitochondrial lipoic acid scavenging is essential for Plasmodium berghei liver stage development. *Cell Microbiol* **14**, 416-430 (2012). https://doi.org:10.1111/j.1462-5822.2011.01729.x

50 Vijayan, K. *et al.* A genome-wide CRISPR-Cas9 screen identifies CENPJ as a host regulator of altered microtubule organization during Plasmodium liver infection. *Cell Chem Biol* **29**, 1419-1433 e1415 (2022). https://doi.org:10.1016/j.chembiol.2022.06.001

51 Eisenberg-Bord, M. *et al.* Cnm1 mediates nucleus-mitochondria contact site formation in response to phospholipid levels. *J Cell Biol* **220** (2021). https://doi.org:10.1083/jcb.202104100

52 Kakimoto, Y. *et al.* Visualizing multiple inter-organelle contact sites using the organelle-targeted split-GFP system. *Sci Rep* **8**, 6175 (2018). https://doi.org:10.1038/s41598-018-24466-0

53 Nagaoka, M. *et al.* The Orphan Nuclear Receptor NR4A3 Is Involved in the Function of Dendritic Cells. *J Immunol* **199**, 2958-2967 (2017). https://doi.org:10.4049/jimmunol.1601911

54 Swanson, K. V., Deng, M. & Ting, J. P. The NLRP3 inflammasome: molecular activation and regulation to therapeutics. *Nat Rev Immunol* **19**, 477-489 (2019). https://doi.org:10.1038/s41577-019-0165-0

55 Afriat, A. *et al.* A spatiotemporally resolved single-cell atlas of the Plasmodium liver stage. *Nature* **611**, 563-569 (2022). https://doi.org:10.1038/s41586-022-05406-5

56 Bertolino, P. & Bowen, D. G. Corrigendum: Malaria and the liver: immunological hide-and-seek or subversion of immunity from within? *Front Microbiol* **6**, 460 (2015). https://doi.org:10.3389/fmicb.2015.00460

57 Goud, B., Liu, S. & Storrie, B. Rab proteins as major determinants of the Golgi complex structure. *Small GTPases* **9**, 66-75 (2018). https://doi.org:10.1080/21541248.2017.1384087

58 Hunter, C. A. & Sibley, L. D. Modulation of innate immunity by Toxoplasma gondii virulence effectors. *Nat Rev Microbiol* **10**, 766-778 (2012). https://doi.org:10.1038/nrmicro2858

59 Stanway, R. R. *et al.* Genome-Scale Identification of Essential Metabolic Processes for Targeting the Plasmodium Liver Stage. *Cell* **179**, 1112-1128.e1126 (2019). https://doi.org:10.1016/j.cell.2019.10.030

60 Dow, G. S. *et al.* Radical curative efficacy of tafenoquine combination regimens in Plasmodium cynomolgi-infected Rhesus monkeys (Macaca mulatta). *Malar J* **10**, 212 (2011). https://doi.org:10.1186/1475-2875-10-212

61 Baird, J. K. 8-Aminoquinoline Therapy for Latent Malaria. *Clin Microbiol Rev* **32** (2019). https://doi.org:10.1128/CMR.00011-19

62 Roth, A. *et al.* A comprehensive model for assessment of liver stage therapies targeting Plasmodium vivax and Plasmodium falciparum. *Nat Commun* **9**, 1837 (2018). https://doi.org:10.1038/s41467-018-04221-9

978 63 Janse, C. J. *et al.* High efficiency transfection of Plasmodium berghei facilitates novel
979 selection procedures. *Molecular and Biochemical Parasitology* **145**, 60-70 (2006).
980 https://doi.org:10.1016/j.molbiopara.2005.09.007

981 64 Rosenberg, R., Wirtz, R. A., Schneider, I. & Burge, R. An estimation of the number of
982 malaria sporozoites ejected by a feeding mosquito. *Trans R Soc Trop Med Hyg* **84**, 209-
983 212 (1990). https://doi.org:10.1016/0035-9203(90)90258-g

984 65 Medica, D. L. & Sinnis, P. Quantitative dynamics of Plasmodium yoelii sporozoite
985 transmission by infected anopheline mosquitoes. *Infect Immun* **73**, 4363-4369 (2005).
986 https://doi.org:10.1128/IAI.73.7.4363-4369.2005

987 66 Sattabongkot, J. *et al.* Establishment of a human hepatocyte line that supports in vitro
988 development of the exo-erythrocytic stages of the malaria parasites Plasmodium
989 falciparum and P. vivax. *Am J Trop Med Hyg* **74**, 708-715 (2006).

990 67 Swann, J. *et al.* High-Throughput Luciferase-Based Assay for the Discovery of
991 Therapeutics That Prevent Malaria. *ACS Infect Dis* **2**, 281-293 (2016).
992 https://doi.org:10.1021/acsinfecdis.5b00143

993 68 Yalaoui, S. *et al.* Hepatocyte permissiveness to Plasmodium infection is conveyed by a
994 short and structurally conserved region of the CD81 large extracellular domain. *PLoS*
995 *Pathog* **4**, e1000010 (2008). https://doi.org:10.1371/journal.ppat.1000010

996 69 Silvie, O. *et al.* Expression of human CD81 differently affects host cell susceptibility to
997 malaria sporozoites depending on the Plasmodium species. *Cell Microbiol* **8**, 1134-1146
998 (2006). https://doi.org:10.1111/j.1462-5822.2006.00697.x

999 70 Prudencio, M., Rodriguez, A. & Mota, M. M. The silent path to thousands of merozoites:
1000 the Plasmodium liver stage. *Nature reviews. Microbiology* **4**, 849-856 (2006).
1001 https://doi.org:10.1038/nrmicro1529

1002 71 Love, M. I., Huber, W. & Anders, S. Moderated estimation of fold change and dispersion
1003 for RNA-seq data with DESeq2. *Genome Biol* **15**, 550 (2014).
1004 https://doi.org:10.1186/s13059-014-0550-8

1005 72 Bahamontes-Rosa, N. *et al.* New molecular settings to support in vivo anti-malarial assays.
1006 *Malar J* **15**, 147 (2016). https://doi.org:10.1186/s12936-016-1205-x

1007 73 Moreno, M. *et al.* Infection of laboratory-colonized Anopheles darlingi mosquitoes by
1008 Plasmodium vivax. *Am J Trop Med Hyg* **90**, 612-616 (2014).
1009 https://doi.org:10.4269/ajtmh.13-0708

1010 74 Moreno, M. *et al.* Continuous Supply of Plasmodium vivax Sporozoites from Colonized
1011 Anopheles darlingi in the Peruvian Amazon. *ACS Infect Dis* **4**, 541-548 (2018).
1012 https://doi.org:10.1021/acsinfecdis.7b00195

75 Franke-Fayard, B. *et al.* Simple and sensitive antimalarial drug screening in vitro and in vivo using transgenic luciferase expressing Plasmodium berghei parasites. *Int J Parasitol* **38**, 1651-1662 (2008). https://doi.org:10.1016/j.ijpara.2008.05.012

1031 **FIGURE LEGENDS**

1032 **Figure 1**. ***HsNR4A3* is highly upregulated during *Plasmodium* exoerythrocytic infection. a.**
1033 Schematic representation for culture, sorting by FACs, dual RNA Seq and confocal microscopy
1034 strategies, **b.** Volcano plot of differently expressed genes, gene-expression pattern vs *p* value, with
1035 the position of *HsMUC13, HsCGA, HsSLC22A8, HsMALAT1, HsRASSF9, HsSDHA,*
1036 *HsSLC25A27, HsNEAT1, HsTAS2R4*, *HsCXCL2,* and *HsNR4A3* genes indicated at 24 and 48hpi.
1037 **c.** RT-qPCR of *HsMUC13, HsCGA, HsSLC22A8, HsMALAT1, HsRASSF9, HsSDHA,*
1038 *HsSLC25A27, HsNEAT1, HsTAS2R4,* and *HsNR4A3* at 48hpi in the indicated cell lines. *HsSDHA*
1039 was used as a control. Relative expression is presented as a ratio of Infected:Uninfected and
1040 determined using the normalized ΔCT method (data presented as mean ± s.e.m, *n*=3 with
1041 individual biological replicates overlaid, * = *p* value 0.05, ** = *p* value 0.001, *** = *p* value 0.0001,
1042 **** = *p* value <0.0001. *p* values determined by two-tailed *t* test). Data from LaMonte et al.[17].

1043 **Figure 2. Immunofluorescence micrographs of *Plasmodium*-infected cells with human**
1044 **HsNR4A3, HsCGA, HsGOLGA8A, and HsMUC13 antibodies.** Representative confocal
1045 microscopy images of **a.** HC-04 liver cells infected with *P. berghei* parasites 48hpi; **b.** primary
1046 hepatocytes infected with *P. falciparum* parasites 120hpi; **c.** HC-04 liver cells infected with *P.*
1047 *vivax* schizonts forms 120hpi; and **d.** HC-04 liver cells infected with *P. vivax* hypnozoites 120hpi.
1048 Cells were labeled using the next set of antibodies: α-HsNR4A3 (#TA804893), α-HsCGA (#LS-
1049 C293331), α-HsGOLGA8A (#PA5-35036), or α-HsMUC13 (#Ab65109), and visualized with a
1050 goat α-mouse or goat α-rabbit secondary antibody (Alexa Fluor 488 – Green); *P. vivax*, *P.*
1051 *falciparum* EEFs (b, c, d) were labeled using α-PvUIS4, and *P. berghei* EEFs (a) were labeled
1052 using α-PbUIS4 (#LS-C204260), and visualized with a goat α-mouse and bovine α-goat secondary
1053 antibody (Rhodamine-red), respectively. Nuclei were labeled with DAPI (blue). Merged images
1054 between HsNR4A3, HsCGA, HsGOLGA8A, HsMUC13, PvUIS4, DAPI, and Cell Membrane are
1055 shown. Scale bars 10µm; 63× oil objective.

1056 **Figure 3: Relocation of the HsNR4A3 protein in HC-04 cells infected with *P. berghei***
1057 **parasites in different periods (3-96hpi). a.** Micrographs show HC-04 cells infected with *P.*
1058 *berghei* sporozoites, fixed at different times (3, 6, 12, 18, 24, 48, 72, and 96 hours). Cells were
1059 labeled using a α-HsNR4A3 (#TA804893) and visualized with a goat α-mouse secondary antibody

1060 (Rhodamine – red); CellMask deep red was used for plasma membranes (Cell Membrane -
1061 magenta). *P. berghei* parasites were labeled using α-PbUIS4 (#LS-204260) and visualized with a
1062 bovine α-goat secondary antibody (Alexa Fluor 488 - green). Nuclei were labeled with DAPI
1063 (blue). Merged images between HsNR4A3, PbUIS4, DAPI, and Cell Membrane are shown. Scale
1064 bars 10μm; 63× oil objective. **b.** Schematic representation of HsNR4A3 relocalization during
1065 *Plasmodium* exoerythrocytic infection in infected and uninfected liver cells.

1066 **Figure 4. U-ExM on huh7.5.1 cells infected with *P. berghei* parasites shows HsNR4A3 protein**
1067 **at the PVM.** Five representative micrographs show Huh7.5.1 cells after 48h of infection with *P.*
1068 *berghei* parasites prepared for U-ExM (see Methods), stained with a nuclear stain (Sytox Deep
1069 Red in cyan), α-PbUIS4 (in magenta), α-HsNR4A3 (in yellow) and a protein stain (NHS-ester, in
1070 grayscale) and visualized using Airyscan 2 microscopy. Yellow arrows indicate concentration of
1071 HsNR4A3 in pockets associated with the PVM. Scale bars as labelled in each image, solid bar =
1072 XY scale and all images are Z-projection with a combined depth of slices of 0.39 μm

1073 **Figure 5. Relocation of HsCXCL2 protein in HC-04 cells infected with *P. berghei* parasites**
1074 **in different periods (2, 24, and 48hpi). a.** Micrographs show HC-04 cells infected with *P. berghei*
1075 parasites, treated with LPS (1μg/ml), fixed, and stained using IFA and confocal microscopy. Cells
1076 were labeled using α-HsCXCL2 (#PA5-80529) and visualized with a donkey α-rabbit secondary
1077 antibody (Rhodamine, red); CellMask deep red was used for plasma membranes (Cell Membrane
1078 - magenta). *P. berghei* parasites were labeled using α-PbUIS4 (#LS-204260) and visualized with
1079 a donkey α-goat secondary antibody (Alexa Fluor 488, green). Nuclei were labeled with DAPI
1080 (blue). Merged images between HsCXCL2, PbUIS4, DAPI and Cell Membrane are shown. Scale
1081 bars 10μm; 63× oil objective. Antibody controls (no α-HsCXCL2, no α-PbUIS4) and uninfected
1082 cells with and without LPS treatment are shown. Scale bars 10μm; 63× oil objective. **b.** Pearson's
1083 correlation coefficient (PCC) between α-PvUIS4 and α-HsCXCL2 staining. Images were analyzed
1084 with Volocity 3D/4D Rendering Software, and PCC was calculated for identified objects. Each
1085 point represents one infected cell from one of three biological replicates. Data were analyzed with
1086 a two-tailed *t* test, ** = $p < 0.05$, **** = $p < 0.0001$.

1087

1088

1089

1090

1091

1092

1093

1094

1095

1096

1097

1098

1099

1100

1101

1102

1103

1104

1105

1106

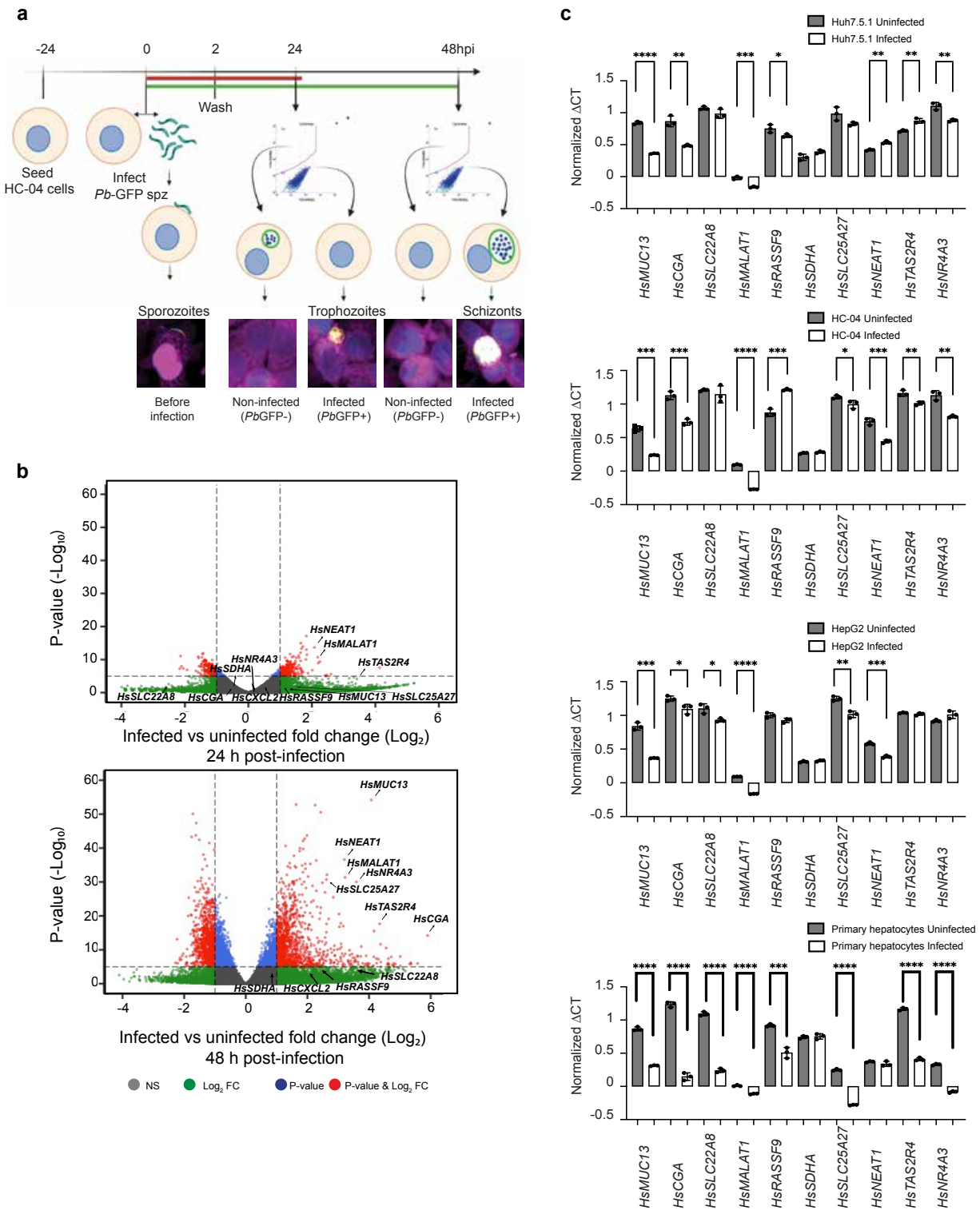

1107 Figure 1

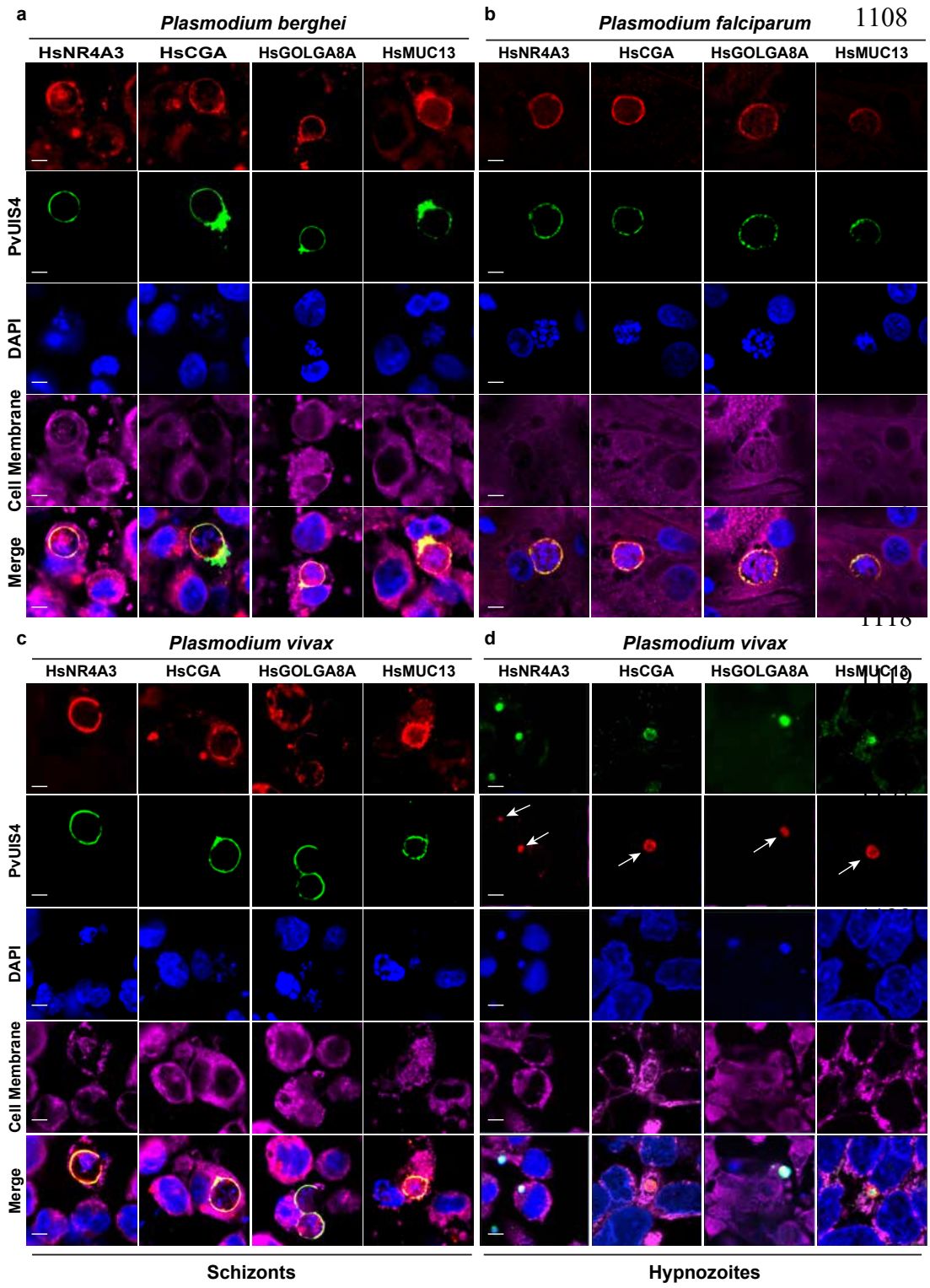
a
Plasmodium berghei
b
Plasmodium falciparum
c
Plasmodium vivax
d
Plasmodium vivax
HsNR4A3
HsCGA
HsGOLGA8A
HsMUC13
PvUIS4
DAPI
Cell Membrane
Merge
Schizonts
Hypnozoites

Figure 2

1132

1133

1134

1135

1136

1137

1138

1139

1140

1141

1142

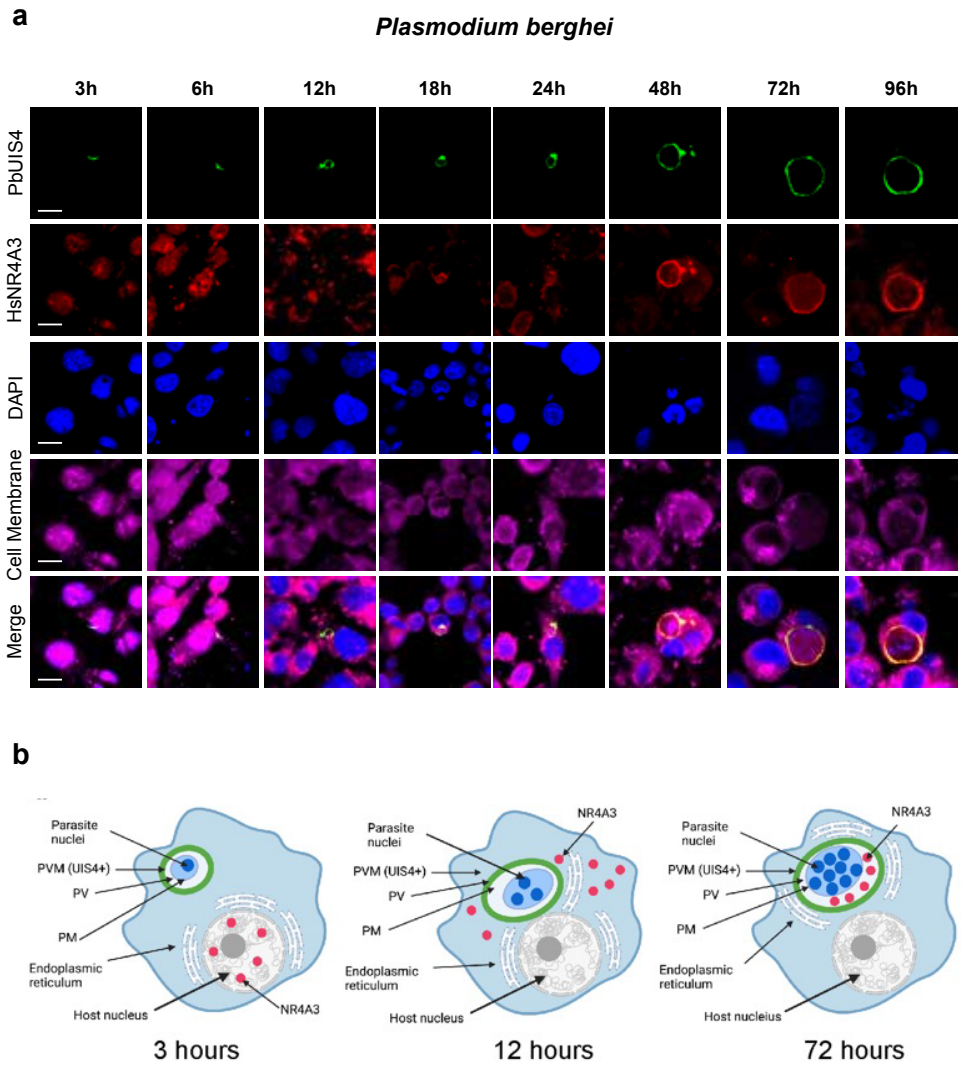

1143

1144

1145

1146

1147

1148

1149

1150

1151 Figure 3

1152

1153

1154

1155

1156

1157

1158

1159

1160

1161

1162

1163

1164

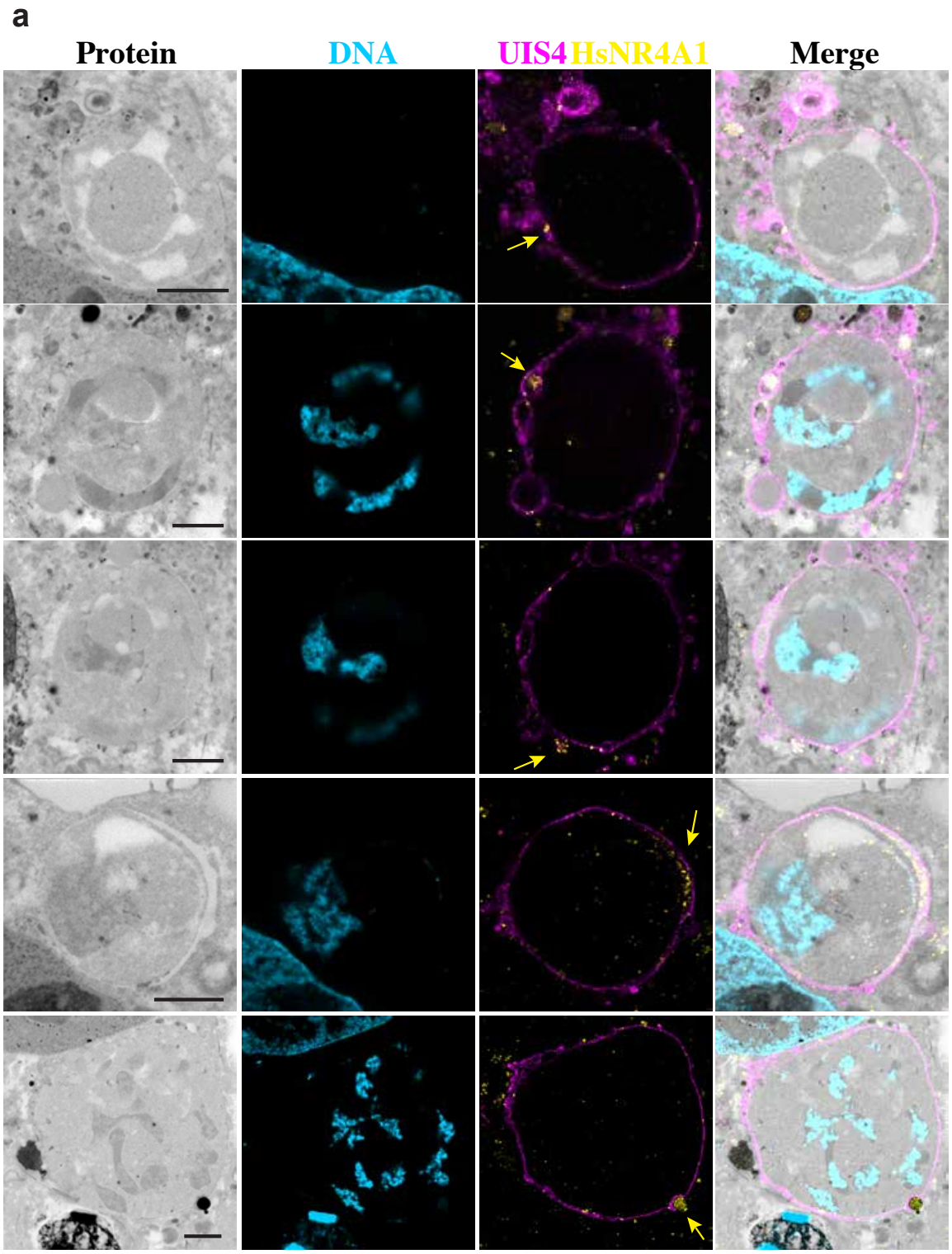

1165 Figure 4

1166

1167

1168

1169

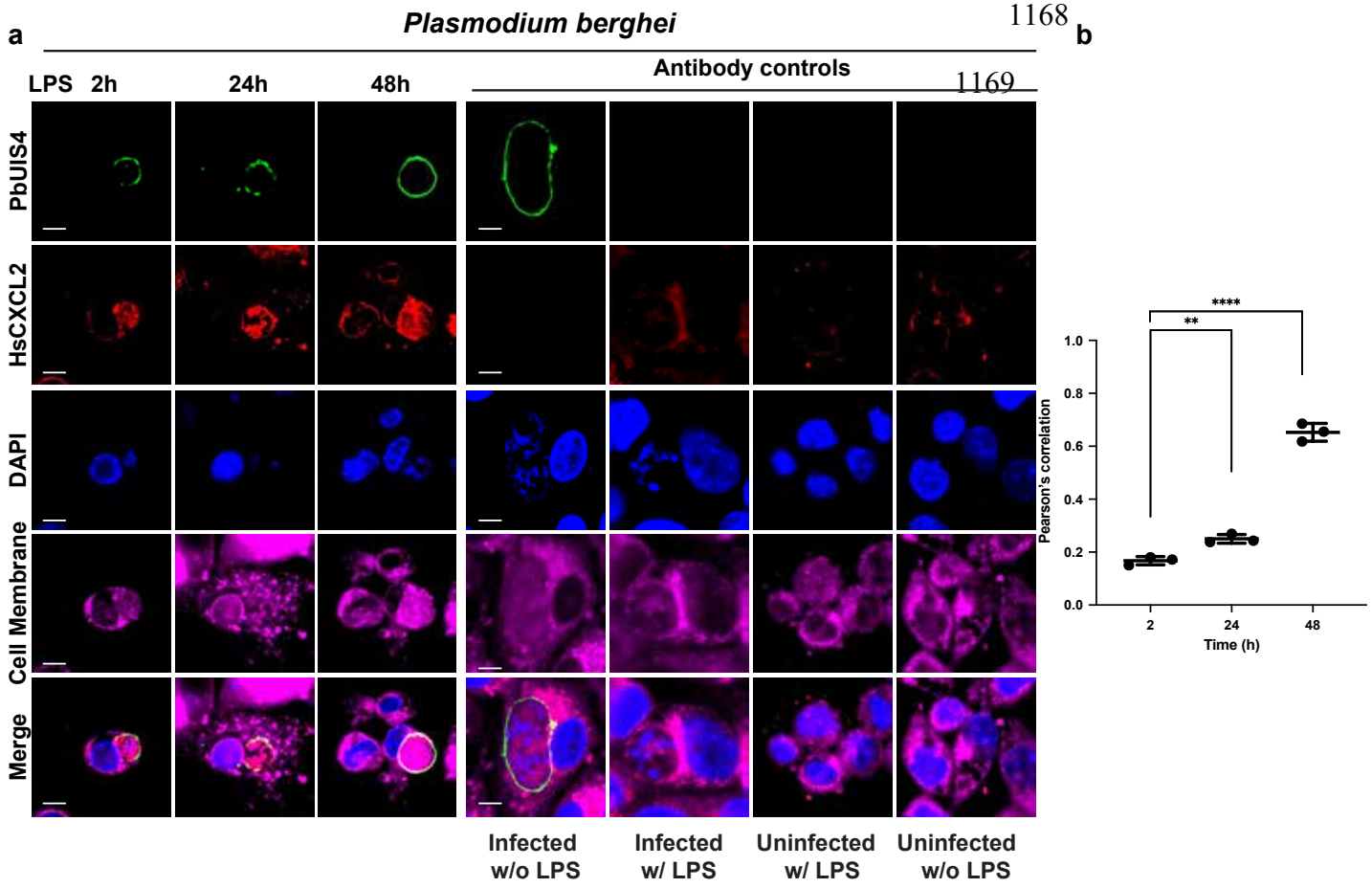

1174

1175

1176

1177 Figure 5

1178

1179